McKelvey School of Engineering Theses & Dissertations

McKelvey School of Engineering

Winter 12-2023

An Apparatus to Quantify Lengthwise Flexural Rigidity Profiles of Endovascular Devices

Charles B. Suskin
Washington University – McKelvey School of Engineering

Follow this and additional works at: https://openscholarship.wustl.edu/eng_etds

Part of the Applied Mechanics Commons

WASHINGTON UNIVERSITY IN ST. LOUIS

McKelvey School of Engineering
Department of Mechanical Engineering & Materials Science

Thesis Examination Committee:
Guy M. Genin, Co-Chair
Joshua W. Osbun, Co-Chair
Matthew R. Bersi
Mohamed A. Zayed

An Apparatus to Quantify Lengthwise Flexural Rigidity Profiles of Endovascular Devices
by
Charles B. Suskin

A thesis presented to
the McKelvey School of Engineering
of Washington University in
partial fulfillment of the
requirements for the degree
of Master of Science

December 2023
St. Louis, Missouri

Table of Contents

List of Figures

List of Tables

List of Abbreviations

EI Flexural rigidity

TFA Transfemoral access

TRA Transradial access

Acknowledgments

I would like to thank Drs. Guy Genin, Joshua Osbun, and Mohamed Zayed for their support throughout my research, along with the other members of this team: Michael Qiu, DeVaughn Rucker, Dr. Sophie Roberts, Juan Becerra-Garcia, Zya Zheng, Karan Joseph, Sheriden (Birdie) Lee, and Avi Hari. In particular, I would like to thank Juan Becerra-Garcia for his work on data acquisition and processing. Additional thanks to Chase Hartquist, Jin Vivian Lee, Vinay Chandrasekaran, and Halle Lowe for their work on *Stability of navigation in catheter-based endovascular procedures* before Michael and I joined, and to Dr. Eric Leuthardt in addition to Chase, Vinay, and Halle for their work on *Quantification of the flexural rigidity of peripheral arterial endovascular catheters and sheaths.*

Thank you Guy for supporting me since I first took Dynamics with you. If it weren't for you, I would not have gotten started in academic research with such a supportive group of collaborators and mentors, for which I am forever grateful.

Thank you Dr. Osbun for your continued support throughout this project. Your manner of describing procedures and device behavior is truly remarkable and at the center of a lot of the developments that our team has made over the last year-and-a-half.

Thank you Dr. Bersi for taking the time to sit on my thesis defense committee and being a valuable voice when I sought advice over the past few years.

Thank you Dr. Zayed for your faith in trying out our ideas. The support that you've shown for turning ideas into reality and in our testing has been incredible.

Thank you Michael for being a truly great collaborator since we joined this team together.

<div align="right">

Charles B. Suskin

</div>

Washington University in St. Louis
December 2023

My thesis is dedicated to my parents, sister, and grandparents. Dad, it feels nice to be able to put you in my dedication section for the first time. Mom, thanks for always fostering my random building impulses.

ABSTRACT OF THE THESIS

An Apparatus to Quantify Lengthwise Flexural Rigidity Profiles of Endovascular Devices

by

Charles B. Suskin

Master of Science in Mechanical Engineering

Washington University in St. Louis, 2023

Professor Guy M. Genin, Co-Chair

Associate Professor Joshua W. Osbun, Co-Chair

Endovascular procedures require access to distal anatomical sites through the vasculature using catheters and guidewires. Quantitative frameworks for device behavior during procedures hold the potential to drive device design through greater understanding of the mechanical behavior of endovascular devices, and offer the potential to personalize care based on a patient's particular vascular anatomy. However, data that would facilitate this technology are lacking, partly due to undisclosed material properties from manufacturers and partly due to the intricate variations along the length of each device due to material changes and the intersections between them. We developed a three-point bend test methodology on a custom apparatus to measure lengthwise flexural rigidity profiles of endovascular devices commonly used to target the neurovasculature. The methodology demonstrated high repeatability and was able to characterize transition zones. We applied the method to generate the first comprehensive, quantitative library of device flexural rigidities, spanning guidewires, intermediate guide catheters, and long sheaths. Additional plots examining relationships between flexural rigidity, device diameter, and length reveal application-specific trends in flexural properties. This methodology and the data allow for standardized characterization and comparisons to aid device selection, and have the potential to both enhance surgical planning and inform future innovation.

Chapter 1

Background Information

1.1   Basics of Endovascular Procedures

Endovascular procedures are standard procedures that interventionalists use to treat stenosis, aneurysm, vascular dissection, and thrombosis. These procedures involve introducing a combination of guidewires, catheters, sheaths, and therapeutic devices at a near-surface arterial access point and tracking the devices to a distal target. For neurovascular procedures, the most common two access points are the left femoral artery, called TFA or transfemoral access, and the right radial artery, called TRA or transradial access. For lower extremity peripheral vascular procedures, contralateral femoral artery access is generally the access point, though ipsilateral femoral artery access and tibial artery access are sometimes also utilized.

Femoral access is widely used for a variety of vascular procedures because the artery is very large, easy to access, and allows fairly non-tortuous and close access to most major arteries in the body. For neurovascular procedures, right carotid artery access is fairly simple using TRA, though left carotid artery access requires traversing an unsupported bend to track down the innominate artery, across the aortic arch, and up the left carotid artery. Radial access have been found to have a significant reduction in adverse cardiac events with death down from 9.2% in femoral access to 5.2% in radial access, as well as fewer access site complications, fewer incidents of major bleeding, and shorter lengths of stay in hospitals. [6]

1.2 Herniation as a Clinical and Engineering Problem

One of the key modes of intervention failure is herniation. In herniation, the guidewire or catheter partially cannulates a target vessel around an unsupported bend, but then the device loses access or cannot advance further around the bend. Instead, it drops into the space available in a non-target local branch. Common occurrences of this are herniation into the descending aorta while traversing from one femoral artery to the contralateral side and herniation into the aortic arch, descending aorta, or ascending aorta while traversing from the brachiocephalic trunk to the left carotid. Herniation criteria have been developed by this group in *Stability of navigation in catheter-based endovascular procedures* by Hartquist et. al.[5] These criteria are based on anatomical properties that can be measured from scans and mechanical properties of the endovascular devices.

Using the theory of minimum potential energy, the bending energy stored across both devices in the curve can be determined for both the success shape and herniation shape. After rewriting, the equation takes the form:

$$\frac{(EI)_2}{(EI)_1} \geq 10 \left[\frac{R/r - 2/5}{4 - R/r} \right] \tag{1.1}$$

EI_1 is the first device passed through the anatomy, usually the guidewire, EI_2 is the second device passed through, typically the catheter, R is the radius of the largest unobstructed curve that can be formed between the innominate and the left carotid, and r is the larger value of either the radius of the artery that the device can herniate into or the distance between the right walls of the innominate and the left carotid, as is shown in fig. 1.1. [5] For the sake of usefulness to physicians, there is little benefit to separating the Young's Modulus of the catheter from the area moment of inertia, E and I respectively, because they are selecting items off the shelf and the combined EI is sufficient to describe behavior.

1.3 Goals of this Project

Past attempts to characterize catheter material properties have been underwhelmingly accurate and precise. They have generally used a cantilevered beam method, but these soft devices are not well suited to that method. Viscoelastic behavior leads to variation between

tests in both the initial "at rest" state, as well as the measured deflection based on how long after the load was applied to the device. This means that one device could have two drastically different deflections at different times of the same test. An additional flaw to cantilevered beam testing is that it requires short, light segments of the device to overhang. These devices, however, often have multiple stiffness transitions along their lengths at undisclosed positions, and the mass of the device itself is often significant in how it deflects. Some of these issues can be alleviated using a suspended cantilevered beam, where the endovascular device is pointed downwards instead of horizontally before being deflected laterally, but nevertheless, the remaining problems remain. [4, 7]

For this project, we built and tested a three-point bending apparatus to quantify the lengthwise variation of the flexural rigidity of a variety of devices without permanently damaging any of them.
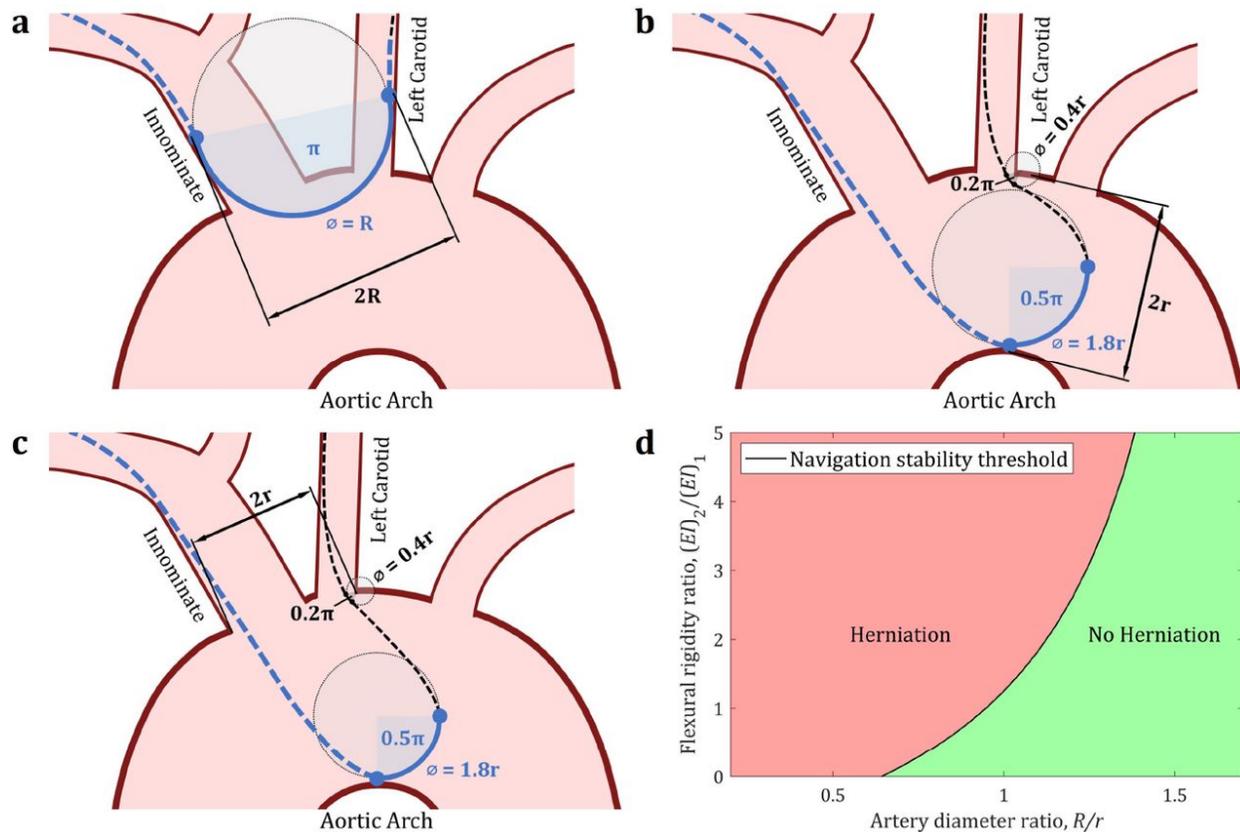
Figure 1.1: **Mathematical models of endovascular navigation stability require knowledge of the mechanical properties of catheters.** (a-c) The difference between successful (a) and unsuccessful (b-c) navigation of a catheter-guidewire system around an aortic arch depends upon patient specific anatomy and the flexural rigidities of the catheters and guidewires. In these schematics, black lines represent the first device, and blue lines represent the coaxial combination of both devices. The regions of high curvature (solid lines) store the highest flexural strain energy. (a) Successful transit of the aortic arch. (b) Herniation, and a schematic of the critical dimension, $2r$ (the aortic arch diameter). (c) Herniation into an aortic arch that is wide relative to the spacing between the innominate and left carotid. Here, $2r$ is instead the distance between the base of the innominate artery and the left carotid artery. (d) A phase diagram for successful navigation depends upon the ratios of device flexural rigidities, and on patient anatomy. [5]

Chapter 2

Three-Point Bend Theory

2.1 Transverse Point Loading of a Simply Supported Beam

The endovascular devices were treated as simply supported linear elastic Euler-Bernoulli beams. The angle of deflection did not exceed the small angle assumption, the devices did not buckle radially, and the application of the load was sufficiently rapid that there was no evidence of viscoelastic relaxation within the test to require additional testing of the viscoelastic time constants for the EI calculations.
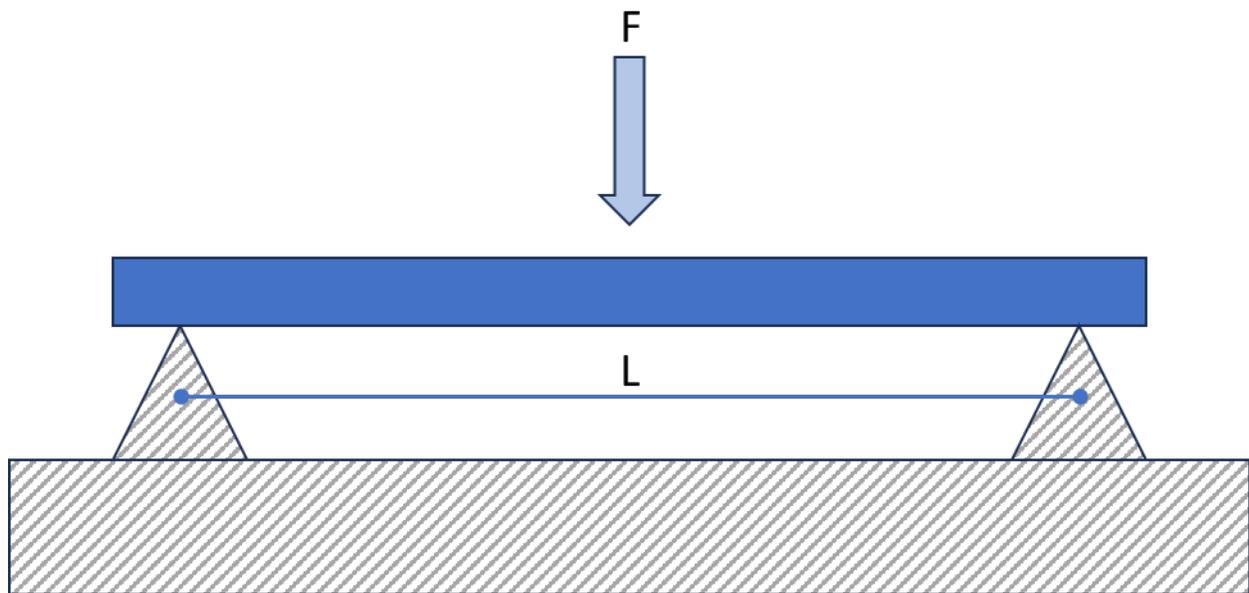
Figure 2.1: **Loading diagram of a three-point bend apparatus.** F is a point load applied to the midpoint between the supports, which are located at positions $x = 0$ and $x = L$, a length L apart.

The problem was defined as shown in fig. 2.1, with a point load in the center of the two supports. Based on these assumptions, the displacement boundary conditions are:

$$v(0) = 0 \tag{2.1}$$

$$v(L) = 0 \tag{2.2}$$

where $v(x)$ is the vertical displacement due to bending at the point x along the axis of the device, and points $x = 0$ and $x = L$ correspond with the locations of the two supports. The load conditions are:

$$q = -F\delta(x - \frac{L}{2}) \tag{2.3}$$

$$M(0) = 0 \tag{2.4}$$

$$M(L) = 0 \tag{2.5}$$

where q is the total load on the device, F is the applied load by the apparatus, L is the length between the supports, and $M(x)$ is the applied moment at a point. The general equation for the displacement of a static deflected beam is:

$$EIv'''' - q = 0 \tag{2.6}$$

where EI is the flexural rigidity, v'''' is the fourth derivative with respect to x, and q is previously defined in eq. 2.3. After integrating and rewriting the flexural rigidity, EI, in terms of L, F, and $v(\frac{L}{2})$, it is found that:

$$EI = \frac{FL^3}{48v(\frac{L}{2})} \tag{2.7}$$

Because it is assumed that the material is linear elastic, it can be further inferred that as the force and deflection change, their proportion should remain constant. Therefore, eq. 2.7 can be further rewritten as:

$$EI = \frac{L^3}{48} \frac{dF}{dv(\frac{L}{2})} \tag{2.8}$$

where $\frac{dF}{dv(\frac{L}{2})}$ is the slope of the force-displacement curve, which is acquired from the testing apparatus.

Chapter 3

Three-Point Bend Apparatus

3.1 CNC Frame

A 3-axis CNC router (Genmitsu 3018-PROVer) was used for the base of the three-point bend device. The CNC gantry was modified by removing the spindle motor to accommodate a custom load cell fixture attached via bolts to the Z-axis carriage. A load cell fixture was made of a combination of 3D printed parts, off-the-shelf components, and machined parts. The Z-axis stepper motor was used to advance and retract the loading pin by raising and lowering the Z-axis carriage.

3.2 Custom Three-Point Bend Test Fixture

A custom three-point bend test fixture was made that attaches to the CNC frame. Two support pins were secured to 3D printed fixtures that bolt down to the bed of the CNC. Additional rollers were attached to the 3D printed fixtures above and slightly offset of the two support pins to assist in aligning the test specimen without affecting the load measurement. Two extruded aluminum rails were then bolted to the bed, one on either side of the two support pins. The inner surface of the extruded rail was lined up with the top of the support pins to allow for a single uniform surface to support the full length of the test specimen. The full test fixture was made and assembled using a combination of 3D printed parts, off-the-shelf components, and machined parts.
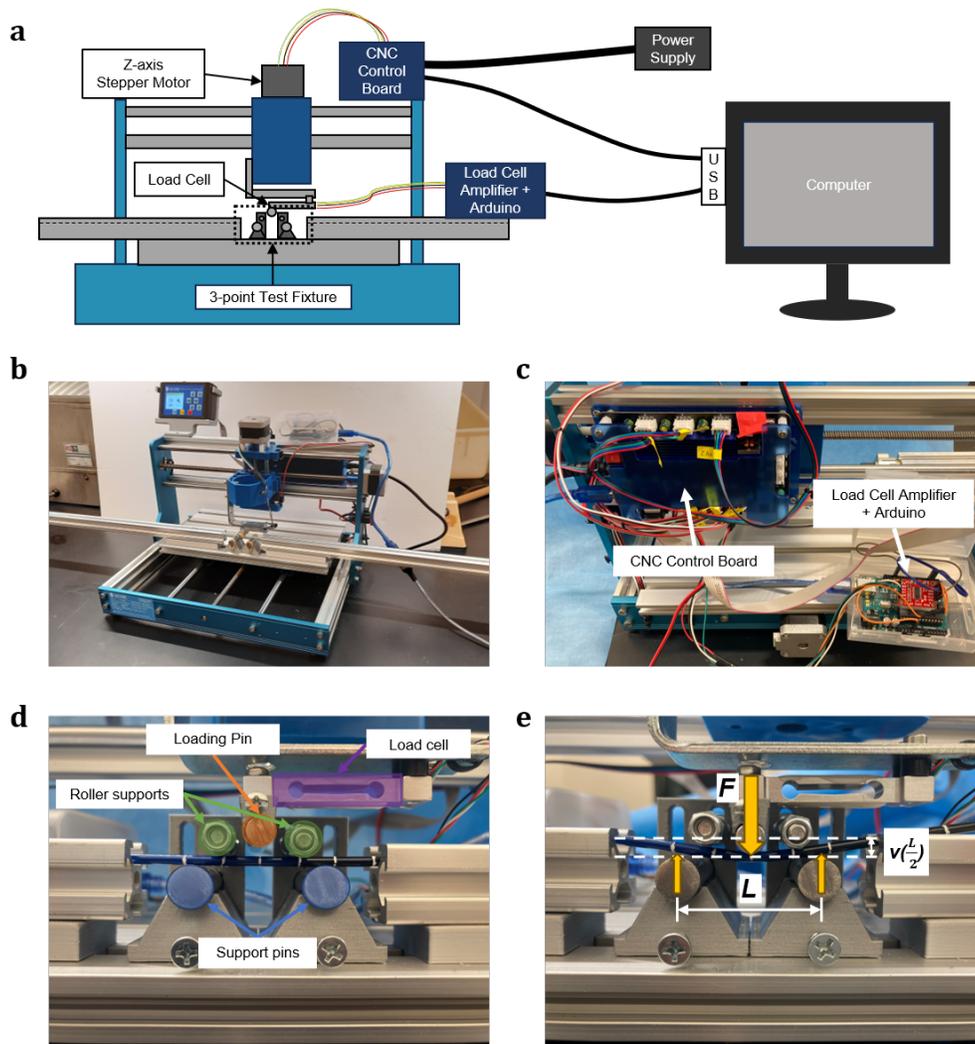
Figure 3.1: **Three-Point Bending Apparatus**: **(a)** Device schematic with electronic components and connections shown. Dashed line along the runners show the location of the bottom of the trench in the extruded aluminum used to align and level the devices. **(b)** Photograph of the apparatus. **(c)** Photograph of the electronic control units and outputs of the apparatus. The CNC control board controls the the Z-axis stepper motor, adjusting the vertical position of the loading pin. The load cell outputs the measured force data to the Arduino based load cell amplifier and data acquisition microcontroller, which outputs the data to computer.**(d)** Enlarged photo of the three point bend test region of the apparatus. The loading pin and load cell are attached to the Z-axis stepper motor, while the roller supports and support pins are rigidly fixed to the chassis. The roller supports provide alignment assistance, but do not contact the devices during the test. **(e)** Photograph of the free body diagram superimposed onto a specimen being tested with loading force (F), distance between support pins (L), displacement of the top of the catheter at the midpoint between the support pins ($v(\frac{L}{2})$) reaction forces at the support pins labeled.

3.3 Load Cell and Control Electronics

The signal from the 500g load cell (Sparkfun TAL221) was amplified using a load cell amplifier (Sparkfun HX711) before being fed into a microcontroller (Arduino Uno Rev3). The load cell was calibrated using the standard method with a series of test weights. Control of the CNC gantry was accomplished using the factory GRBL motor control board included with the 3018-PROVer.

3.4 Control Software

Communication with the device was established over two USB connections: one to the Arduino microcontroller for data acquisition and one to the motor control board for positioning of the loading pin. Motor control was done using G-code scripts executed in the GRBL controller software Candle. Data acquisition was done using PuTTY.

3.5 Measurement Protocol

For each device, starting from the distal end, marks were made at 1 cm increments through the distal transition zones to indicate each test point location. At the main shaft, 5 cm increments were used given that the main shaft has a constant construction. Test points were marked up to 40-55 cm from the distal tip depending on the device and extent of the transition zones. For each test, a test point was centered under the loading pin, which was then lowered at a constant feed rate of 0.5 mm/s for 2 mm. The loading pin was held for 5 seconds, before being retracted. After one test point was measured, the device was manually advanced to the next test point. The force applied by the loading pin as measured by the load cell was recorded continuously using the Arduino microcontroller.

Three-Point Bend Parameters	
Variable	**Value or Source of Measurement**
L	30 [mm]
F	Measured by load cell
$v(\frac{L}{2})$	Output by CNC controller
Z-axis Commands	
Rate [mm/s]	**Duration [s]**
-0.5	4
0.0	5
0.5	4

Table 3.1: **Table of three-point bend apparatus parameters and z-axis commands.**

3.6   Calculation of Flexural Rigidity

Following acquisition of the load cell measurements, the raw force data was used to calculate flexural rigidity using a custom script written in MATLAB. Time stamps for each force measurement were converted to displacements using the known feed rate specified in Candle. The zero of displacement was taken to be the time stamp where the force first increases during each test. From the force-displacement plot, the flexural rigidity was then calculated by finding the slope of the rise in the force peak associated with each test and then plugging that slope into the three-point bend equation for flexural rigidity.

Chapter 4

Device Flexural Rigidity Measurements and Lengthwise Flexural Rigidity Profiles

4.1   Procedure

Endovascular devices were marked at known intervals along their lengths from the distal tip until the device seemed to stop changing its rigidity profile, as shown in fig 4.2. For guidewires, this often occurs between 45 cm and 60 cm from the distal tip. For intermediate guide catheters, a subcategory of catheters, this often occurs between 40 cm and 50 cm from the distal tip. For long sheaths, another subcategory of catheters, this often occurs between 37 cm and 45 cm from the distal tip. Regions beyond these lengths are also less clinically relevant because the more proximal zones are unlikely to reach the unsupported bend, especially in neurointerventional cases, where the catheter and sheath rarely progress beyond the termination of the left common carotid artery, which is usually no longer than 13.8 cm. [3] The intervals were as low as 1 cm for regions with increasingly varied flexural rigidity and up to 5 cm for zones that held fairly consistent.

The load cell begins a small distance above the device, then lowers at a constant rate for 5 seconds until it is 2 mm from its initial position, held there for 5 seconds, then raised.

4.2   Figures
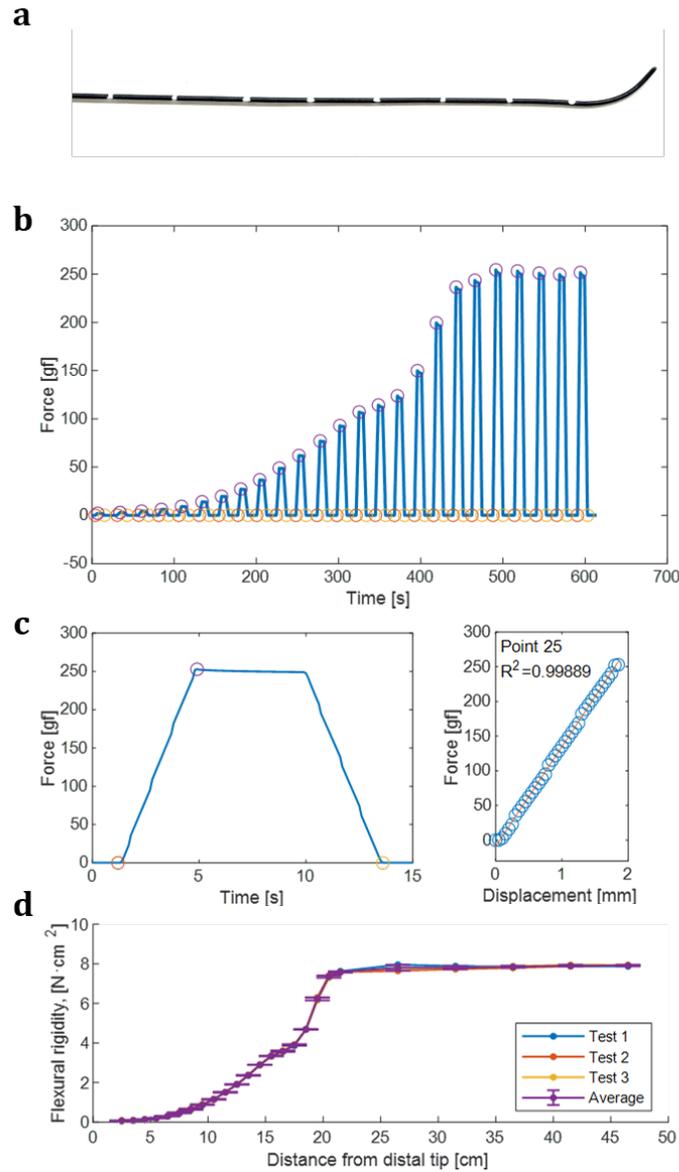
Figure 4.1: **Sample Data: Stiff Roadrunner Guidewire (a)** Photograph of the distal tip of the guidewire with 1 cm intervals marked. **(b)** Force-time graph from the load cell. Initial contact between the catheter and load cell, peak, and loss of contact with the catheter are all circled. **(c)** Enlarged segment of the force-time graph in (a) and a force-displacement graph using the known positions of the load cell from the time-coded CNC control board logs. The slope of the force-displacement graph is the flexural rigidity. **(d)** The lengthwise flexural rigidity profile of the stiff roadrunner guidewire with three tests and the average shown.
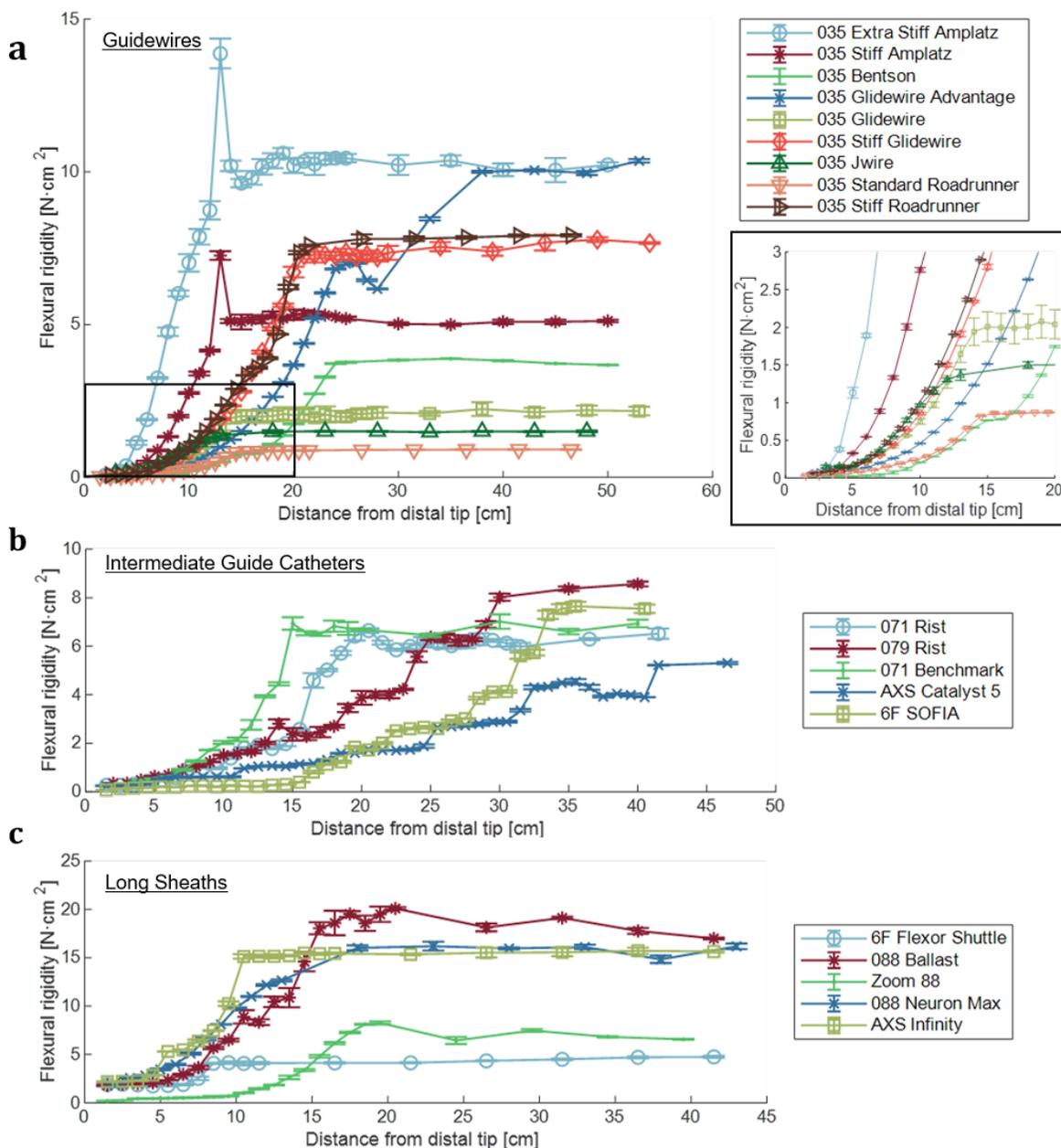
Figure 4.2: **Lengthwise Flexural Rigidity Plots Grouped by Device Type (a)** Lengthwise flexural rigidity plot of 0.035" diameter guidewires with a magnified section of the plot showing greater detail of the range $EI : [0, 3]$; and the distance from the distal tip is: $[0, 20]$. **(b)**Lengthwise flexural rigidity plot of intermediate guide catheters. **(c)** Lengthwise flexural rigidity plot of long sheaths.

Figure 4.3: **Ashby Plot of the Flexural Rigidity of the Proximal End Versus the Distal End** Traditional classifications for devices generally translate into distinct flexural rigidity groupings. Ashby plot showing distal-proximal flexural rigidity relationships for the different devices colored by classification. Devices of each classification occupy a distinct region of the plot. The 6F SOFIA and Zoom 88 are outliers that cross the boundaries of traditional device classifications with distinctly lower distal flexural rigidities. Note that the x-axis is log-scaled.

Figure 4.4: **Ashby Plots of Proximal and Distal Flexural Rigidities Versus Device Outer Diameter** Device outer diameter typically corresponds with traditional device classification. **(a)** Ashby plot showing the relationship between device outer diameter and distal flexural rigidity for the different device classifications. Long sheaths tend to be the largest devices, followed by intermediate guide catheters, and then guidewires. Distal flexural rigidity generally increases with device outer diameter. Note that the y-axis is log-scaled. **(b)** Ashby plot showing the relationship between device outer diameter and proximal flexural rigidity for the different device classifications. Guidewires span nearly the full range of proximal flexural rigidities. Intermediate guides catheters occupy the middle of the range, while long sheaths occupy the middle to extreme high end.

	Distal Flexural Rigidity [N·cm²]	±	Proximal Flexural Rigidity [N·cm²]	±	Distal OD [in]	Proximal OD [in]
		Guidewires				
0.035 Glidewire	0.06	0.001	2.13	0.142	0.035	0.035
0.035 Stiff Glidewire	0.10	0.001	7.67	0.029	0.035	0.035
0.035 Glide Advantage	0.04	0.003	10.36	0.056	0.035	0.035
0.035 Stiff Amplatz	0.06	0.009	5.09	0.045	0.035	0.035
0.035 Extra Stiff Amplatz	0.07	0.012	10.07	0.088	0.035	0.035
0.035 Standard Roadrunner	0.03	0.003	0.91	0.003	0.035	0.035
0.035 Stiff Roadrunner	0.04	0.001	3.96	0.018	0.035	0.035
0.035 Bentson	0.02	0.007	3.68	0.015	0.035	0.035
0.035 Jwire	0.15	0.027	1.50	0.031	0.035	0.035
		Intermediate Guide Catheters				
0.071 Rist	0.27	0.005	6.41	0.210	0.079	0.079
0.079 Rist	0.35	0.010	8.57	0.099	0.092	0.092
0.071 Benchmark	0.28	0.011	6.94	0.158	0.066	0.066
AXS Catalyst 5	0.24	0.008	5.22	0.018	0.070	0.074
6F SOFIA	0.08	0.003	7.54	0.174	0.079	0.079
		Long Sheaths				
Zoom 88	0.21	0.014	6.57	0.039	0.106	0.110
AXS Infinity	2.20	0.013	15.53	0.117	0.105	0.105
0.088 Neuron Max	1.82	0.187	16.18	0.295	0.108	0.108
0.088 Ballast	1.81	0.061	17.00	0.091	0.100	0.106
6F Flexor Shuttle	1.88	0.181	4.75	0.109	0.079	0.079

Table 4.1: **Distal and proximal flexural rigidities along with outer diameters of all devices tested.** The distal value was taken from the test point closest to the distal tip. The proximal values were taken from a test point on the main shaft approximately 40-50 cm from the distal tip depending on device. Outer diameters were referenced from manufacturer's specifications.

4.3   Discussion

The testing methodology for quantifying the lengthwise flexural rigidity of endovascular surgical devices was applied to compile the first publicly-available, comprehensive library of lengthwise flexural rigidity profiles for commercially available neuroendovascular surgical devices used for neurovascular procedures such as stroke. The test rig was assembled using off-the shelf parts, making it both relatively inexpensive and intuitive to use, and has the additional advantage that it can accommodate testing of long specimens. Other methodologies require either cutting the device into short segments[2, 4] or limiting testing to small segments of a catheter.[1] This destructive or spatially limited approaches are especially inconvenient for working with novel, one-off prototypes. By incorporating a rail into the three-point bend fixture, our test rig enables long specimens to be tested non-destructively, and measurements can be taken quickly at any point along their lengths. The test rig utilizes a CNC base and is controlled by G-code, which is industry standard in manufacturing and precision machining, is compatible with a vast library of automation scripts and control

programs, and can be adapted to accommodate additional testing procedures such as cyclic testing or custom load-hold-unload profiles.

Certain limitations with this testing method need to be noted. The linear, Euler-Bernoulli beam theory applied assumes that the geometry of the cross-sections of the beam do not change in a significant manner under load and remain planar to the neutral axis. Solid devices, like guidewires, are unlikely to deform at all under the applied loads, and the hollow devices were monitored and not observed deforming. Linear Euler-Bernoulli theory also implies small-angle deflections, which is valid for the small deflections of $< 2mm$ used in our testing,[1] but would be inaccurate at larger deflections. The theory used to interpret data assumes zero moment at the free ends, and in cases of large overhang by segments of weight that is comparable to the indentation force, accounting for the moment applied by the raised segments beyond either support pin might be warranted. This would likely require density data coupled with optical data to determine the length of the lever arm. Finally, in this study we quantified only the instantaneous flexural rigidity. Viscoelastic effects, in which isometric forces can change in a time dependent manner, were on the order of a few percent for the catheters studied, which is small compared to measurement repeatability. Exploration of strain- or time-dependent mechanical properties can be evaluated using the test rig developed here, and is an avenue for further study.

Most devices were tested three times and averaged, rather than using three different devices. This constraint benefits the validation of the apparatus because testing different devices adds the confounding variables due to possible differences between devices due to manufacturing tolerances. Using the same device for multiple tests allows the precision and harmlessness of the device to be verified. The average magnitude percent difference between the average and corresponding measured values was 2.31%, which shows that the measurements were extremely precise and that the devices behaved the same across tests, meaning that they were not damaged.

The data acquired in this study demonstrated that endovascular surgical devices possess widely varying flexural rigidity properties, including differences in the number and nature of their transition zones and the stiffness of their main shafts. Generally, distal flexural rigidity increased with increasing outer diameter (fig. 4.3). For both distal and proximal flexural rigidity, intermediate guide catheters and sheaths tracked along the same range of scale lines (gray, dashed lines in fig. 4.4), which are isoclines for self-similar catheters of with identical

material properties but different outer diameter. These lines scale as the outer diameter raised to the fourth power, and reveal the effects impact of differences in catheter thickness and selection. Guidewires are often made of metal wires, and lie on isoclines far above both distal and proximal stiffnesses of intermediate guide catheters and sheaths.

Understanding the flexural rigidity profiles of endovascular devices is paramount for successful clinical management of neurovascular pathologies such as stroke. During these procedures, time is often of the essence in order to recover appropriate blood flow to the brain penumbra. Extended endovascular navigation, or repeated challenges in gaining stable access to the distal neurovascular structure of interest can lead to delay in treatment and lasting consequences to the patient. While interventionalists rely heavily on their past experiences and clinical pattern recognition, patient anatomy is highly variable, and no one patient ever has the same vascular anatomy as another. As such subjective assessments can sometimes be misleading, and often require 'on-the-spot' creative ways to treat the patient. Additionally, catheter herniation in of itself can lead to arterial trauma and dissection. The sudden jolt of force exerted by the catheter as it herniates out of a distal vascular structure can damage the sensitive vascular wall, further complicating the procedure and increase the risk of negative perioperative consequences.

Understanding the standard flexural rigidity properties of endovascular devices can enhance personalization of endovascular procedures for specific patient vascular anatomies. Supporting this concept, we observed that guidewires grouped together on the lower end of the distal flexural rigidity range. Functionally, this is expected because guidewires are typically advanced into the narrow vessels and used to select vessels and cross lesions, meaning that they must have soft flexible tips. The proximal flexural rigidities of the main shafts of guidewires spanned a wide range, giving options for more choices to interventionalists. Such a range of properties is desirable as an interventionalist chooses devices to, for example, cross tortuous vasculature or provide more stiffness for added support. Intermediate guide catheters attempt to balance support and flexibility, and occupied the middle range of the Ashby plots (fig. 4.3). Most sheaths were substantially stiffer than guidewires and intermediate guide catheters at their distal ends, with proximal flexural rigidities ranging from the middle to the extreme high end of the range. This corresponds functionally as long sheaths prioritize support over flexibility.

Chapter 5

Conclusion

Our study findings offer a comprehensive, quantitative assessment of the endovascular devices available, which may help with more informed, consistent, and optimized device selection during neurovascular procedures. These quantitative data could also potentially be used to inform future research and innovation. Preliminarily, the Ashby plots highlight openings in the design space that could be filled by new devices, giving interventionalists more options. Quantitative flexural rigidity data are also essential for the development of physics models aiming to explain the mechanics of endovascular device navigation as well as algorithms underlying robotic endovascular surgery platforms. Upon further investigation of the underlying mechanics of these coaxial endovascular interventional systems, intentional placement of zones of particular flexural rigidities can be developed, and complete systems of guidewires, intermediate guide catheters, and long sheaths can be designed and optimized for specific procedures and anatomies. Furthermore, these data, combined with models for navigation, may contribute to automated device selection based on patient-specific anatomy.

References

[1] ASTM International. Standard guide for three-point bending of balloon-expandable vascular stents and stent systems. ASTM F2606-08(2021), 2021.

[2] C. Brandt-Wunderlich, N. Grabow, K.-P. Schmitz, S. Siewert, and W. Schmidt. Cardiovascular catheter stiffness–a static measurement approach. *Current Directions in Biomedical Engineering*, 7(2):721–723, 2021.

[3] F. A. Choudhry, J. T. Grantham, A. T. Rai, and J. P. Hogg. Vascular geometry of the extracranial carotid arteries: an analysis of length, diameter, and tortuosity. *Journal of Neurointerventional Surgery*, 8(5):536–540, May 2016.

[4] C. M. Hartquist, V. Chandrasekaran, H. Lowe, E. C. Leuthardt, J. W. Osbun, G. M. Genin, and M. A. Zayed. Quantification of the flexural rigidity of peripheral arterial endovascular catheters and sheaths. *Journal of the Mechanical Behavior of Biomedical Materials*, 119:104459, July 2021.

[5] C. M. Hartquist, J. V. Lee, M. Y. Qiu, C. Suskin, V. Chandrasekaran, H. R. Lowe, M. A. Zayed, J. W. Osbun, and G. M. Genin. Stability of navigation in catheter-based endovascular procedures, June 2023. Pages: 2023.06.02.543219 Section: New Results.

[6] E. Romagnoli, G. Biondi-Zoccai, A. Sciahbasi, L. Politi, S. Rigattieri, G. Pendenza, F. Summaria, R. Patrizi, A. Borghi, C. Di Russo, C. Moretti, P. Agostoni, P. Loschiavo, E. Lioy, I. Sheiban, and G. Sangiorgi. Radial versus femoral randomized investigation in ST-segment elevation acute coronary syndrome: the RIFLE-STEACS (Radial Versus Femoral Randomized Investigation in ST-Elevation Acute Coronary Syndrome) study. *Journal of the American College of Cardiology*, 60(24):2481–2489, Dec. 2012.

[7] O. Stenqvist, I. Curelaru, L. E. Linder, and B. Gustavsson. Stiffness of central venous catheters. *Acta Anaesthesiologica Scandinavica*, 27(2):153–157, Apr. 1983.

Appendix A

Data

Table A.1: **Table of all calculated catheter and guidewire flexural rigidity values.**

Device	x Position $[cm]$	Test 1 $[Ncm^2]$	Test 2 $[Ncm^2]$	Test 3 $[Ncm^2]$	Avg $[Ncm^2]$	Error
		Flexural Rigidity Values of All Devices				
0.035" Bentson	2	0.0283	0.0281	0.0153	0.0239	24.0367
0.035" Bentson	3	0.0232	0.0297	0.0299	0.0276	10.5720
0.035" Bentson	4	0.0227	0.0124	0.0290	0.0214	28.1233
0.035" Bentson	5	0.0159	0.0271	0.0219	0.0216	17.6336
0.035" Bentson	6	0.0396	0.0275	0.0229	0.0300	21.2657
0.035" Bentson	7	0.0190	0.0517	0.0439	0.0382	33.4869
0.035" Bentson	8	0.0530	0.0909	0.0785	0.0741	19.0100
0.035" Bentson	9	0.1005	0.1331	0.1300	0.1212	11.3951
0.035" Bentson	10	0.2077	0.2056	0.2099	0.2078	0.7003
0.035" Bentson	11	0.2870	0.2856	0.2807	0.2845	0.8734
0.035" Bentson	12	0.3819	0.3912	0.3793	0.3842	1.2292
0.035" Bentson	13	0.5028	0.5102	0.5000	0.5044	0.7765
0.035" Bentson	14	0.6650	0.6713	0.6776	0.6713	0.6267
0.035" Bentson	15	0.7596	0.7698	0.7633	0.7642	0.4838
0.035" Bentson	16	0.7782	0.7906	0.7713	0.7800	0.9078
0.035" Bentson	17	0.8705	0.8941	0.8703	0.8783	1.1984
0.035" Bentson	18	1.0720	1.1058	1.0811	1.0863	1.1933
0.035" Bentson	19	1.3504	1.3720	1.3772	1.3665	0.7875
0.035" Bentson	20	1.7325	1.7595	1.7488	1.7469	0.5509
0.035" Bentson	21	2.2497	2.2468	2.2318	2.2428	0.3250
0.035" Bentson	22	2.7343	2.7237	2.7515	2.7365	0.3656
0.035" Bentson	23	3.2641	3.2793	3.3077	3.2837	0.4873
0.035" Bentson	24	3.7292	3.7092	3.7385	3.7256	0.2946
0.035" Bentson	25	3.7470	3.7731	3.7801	3.7667	0.3487
0.035" Bentson	30	3.8391	3.8237	3.8532	3.8387	0.2605
0.035" Bentson	35	3.8810	3.8911	3.8846	3.8856	0.0946
0.035" Bentson	40	3.8319	3.8329	3.7967	3.8205	0.4154
0.035" Bentson	45	3.7346	3.7223	3.7355	3.7308	0.1511
0.035" Bentson	50	3.6965	3.6676	3.6727	3.6789	0.3186
0.035" Extra Stiff Amplatz	2	0.0782	0.0703	0.0555	0.0680	12.2533
0.035" Extra Stiff Amplatz	3	0.1458	0.1120	0.0857	0.1145	18.2398
0.035" Extra Stiff Amplatz	4	0.4005	0.3862	0.3593	0.3820	3.9643
0.035" Extra Stiff Amplatz	5	1.2131	1.0818	1.1026	1.1325	4.7446
0.035" Extra Stiff Amplatz	6	1.9203	1.8714	1.8832	1.8916	1.0102
0.035" Extra Stiff Amplatz	7	3.2628	3.2712	3.2176	3.2506	0.6757
0.035" Extra Stiff Amplatz	8	4.9225	4.6971	4.6744	4.7647	2.2090
0.035" Extra Stiff Amplatz	9	6.1262	5.9461	5.9819	6.0181	1.1981
0.035" Extra Stiff Amplatz	10	7.3562	6.8866	6.8295	7.0241	3.1520
0.035" Extra Stiff Amplatz	11	8.1646	7.7745	7.6893	7.8761	2.4419
0.035" Extra Stiff Amplatz	12	9.0858	8.5457	8.5915	8.7410	2.6300
0.035" Extra Stiff Amplatz	13	14.4150	13.7377	13.4671	13.8733	2.6032
0.035" Extra Stiff Amplatz	14	10.3923	10.0947	10.1009	10.1960	1.2837
0.035" Extra Stiff Amplatz	15	9.6273	9.5001	9.7720	9.6331	0.9612
0.035" Extra Stiff Amplatz	16	9.7196	9.6355	10.0595	9.8049	1.7315
0.035" Extra Stiff Amplatz	17	10.1230	9.9383	10.4399	10.1670	1.7889
0.035" Extra Stiff Amplatz	18	10.2105	10.2351	10.6450	10.3635	1.8106
0.035" Extra Stiff Amplatz	19	10.6682	10.4223	10.7449	10.6118	1.1904
0.035" Extra Stiff Amplatz	20	9.9492	10.2360	10.4327	10.2060	1.6775
		Continued on next page				

Continuation of Table A.1, Flexural Rigidity Values of All Devices						
Device	**x Position** [cm]	**Test 1** [Ncm^2]	**Test 2** [Ncm^2]	**Test 3** [Ncm^2]	**Avg** [Ncm^2]	**Error**
0.035" Extra Stiff Amplatz	21	10.3003	10.2537	10.4744	10.3428	0.8483
0.035" Extra Stiff Amplatz	22	10.3996	9.8523	10.5190	10.2570	2.6301
0.035" Extra Stiff Amplatz	23	10.2324	10.5928	10.4560	10.4271	1.2448
0.035" Extra Stiff Amplatz	24	10.3600	10.4657	10.5264	10.4507	0.5786
0.035" Extra Stiff Amplatz	25	10.2999	10.5625	10.4811	10.4478	0.9441
0.035" Extra Stiff Amplatz	30	9.8495	10.4123	10.4117	10.2245	2.4448
0.035" Extra Stiff Amplatz	35	10.1828	10.4737	10.4632	10.3732	1.2237
0.035" Extra Stiff Amplatz	40	9.8606	10.0706	10.2754	10.0689	1.3787
0.035" Extra Stiff Amplatz	45	9.6072	10.2557	10.3159	10.0596	2.9980
0.035" Extra Stiff Amplatz	50	10.1272	10.2758	10.2821	10.2283	0.6594
0.035" Glidewire Advantage	3	0.0520	0.0509	0.0395	0.0474	11.2171
0.035" Glidewire Advantage	4	0.0666	0.0658	0.0671	0.0665	0.7069
0.035" Glidewire Advantage	5	0.1096	0.1086	0.1086	0.1089	0.3920
0.035" Glidewire Advantage	6	0.1439	0.1389	0.1389	0.1406	1.5819
0.035" Glidewire Advantage	7	0.2017	0.1968	0.1976	0.1987	0.9996
0.035" Glidewire Advantage	8	0.2649	0.2638	0.2624	0.2637	0.3408
0.035" Glidewire Advantage	9	0.3487	0.3410	0.3408	0.3435	1.0135
0.035" Glidewire Advantage	10	0.4593	0.4591	0.4604	0.4596	0.1123
0.035" Glidewire Advantage	11	0.6123	0.6056	0.6041	0.6073	0.5497
0.035" Glidewire Advantage	12	0.7722	0.7755	0.7730	0.7736	0.1645
0.035" Glidewire Advantage	13	0.9986	0.9905	0.9792	0.9894	0.6867
0.035" Glidewire Advantage	14	1.2365	1.2279	1.2412	1.2352	0.3958
0.035" Glidewire Advantage	15	1.5164	1.5114	1.5149	1.5143	0.1239
0.035" Glidewire Advantage	16	1.8485	1.8467	1.8527	1.8493	0.1219
0.035" Glidewire Advantage	17	2.2223	2.2209	2.2120	2.2184	0.1913
0.035" Glidewire Advantage	18	2.6260	2.6407	2.6401	2.6356	0.2431
0.035" Glidewire Advantage	19	3.1056	3.0898	3.1194	3.1049	0.3248
0.035" Glidewire Advantage	20	3.6812	3.6935	3.6487	3.6745	0.4670
0.035" Glidewire Advantage	21	4.4013	4.3800	4.3688	4.3834	0.2728
0.035" Glidewire Advantage	22	5.2276	5.1890	5.1871	5.2013	0.3377
0.035" Glidewire Advantage	23	6.0485	6.0067	6.0502	6.0351	0.3138
0.035" Glidewire Advantage	24	6.8473	6.8140	6.8113	6.8242	0.2258
0.035" Glidewire Advantage	25	7.0334	7.0090	6.9464	6.9963	0.4748
0.035" Glidewire Advantage	26	7.0283	7.0559	6.9950	7.0264	0.2983
0.035" Glidewire Advantage	27	6.4264	6.4904	6.4460	6.4543	0.3733
0.035" Glidewire Advantage	28	6.1582	6.1837	6.1586	6.1668	0.1821
0.035" Glidewire Advantage	33	8.4620	8.5143	8.4075	8.4613	0.4239
0.035" Glidewire Advantage	38	9.9618	10.0157	10.0239	10.0005	0.2576
0.035" Glidewire Advantage	43	10.0386	10.0228	10.0940	10.0518	0.2798
0.035" Glidewire Advantage	48	9.8921	9.9647	10.0281	9.9617	0.4655
0.035" Glidewire Advantage	53	10.2962	10.3974	10.3891	10.3609	0.4164
0.035" Glidewire	3	0.0585	0.0570	0.0593	0.0583	1.4475
0.035" Glidewire	4	0.1008	0.0994	0.0981	0.0994	0.8980
0.035" Glidewire	5	0.1207	0.1575	0.1505	0.1429	10.3418
0.035" Glidewire	6	0.2084	0.2036	0.2191	0.2104	2.7746
0.035" Glidewire	7	0.2949	0.3102	0.2990	0.3014	1.9455
0.035" Glidewire	8	0.4003	0.4333	0.4241	0.4192	3.0078
0.035" Glidewire	9	0.5611	0.5586	0.5714	0.5637	0.9133
0.035" Glidewire	10	0.7180	0.7409	0.7881	0.7490	3.4762
0.035" Glidewire	11	0.9539	0.9474	1.0160	0.9724	2.9870
0.035" Glidewire	12	1.1791	1.3142	1.3326	1.2753	5.0287
0.035" Glidewire	13	1.5221	1.7291	1.6909	1.6474	5.0707
0.035" Glidewire	14	1.7339	2.0759	2.0186	1.9428	7.1688
0.035" Glidewire	15	1.7801	2.1094	2.1363	2.0086	7.5841
0.035" Glidewire	16	1.7817	2.0883	2.1240	1.9980	7.2178
0.035" Glidewire	17	1.7771	1.9959	2.1944	1.9891	7.1049
0.035" Glidewire	18	1.8212	2.0748	2.1350	2.0103	6.2724
0.035" Glidewire	19	1.8307	2.1619	2.2385	2.0770	7.9076
0.035" Glidewire	20	1.8301	2.2116	2.0812	2.0410	6.8863
0.035" Glidewire	21	1.8495	2.3156	2.0245	2.0632	8.1550
0.035" Glidewire	22	1.8370	2.0686	1.9539	1.9532	3.9650
0.035" Glidewire	23	1.8294	2.3426	2.0112	2.0611	9.1065
0.035" Glidewire	24	1.8210	2.1832	1.9804	1.9948	6.2941
0.035" Glidewire	25	1.8411	2.1104	1.9779	1.9765	4.5651
0.035" Glidewire	26	1.9300	2.1441	2.1603	2.0781	4.7525
Continued on next page						

[22]

Continuation of Table A.1, Flexural Rigidity Values of All Devices						
Device	**x Position** [cm]	**Test 1** [Ncm^2]	**Test 2** [Ncm^2]	**Test 3** [Ncm^2]	**Avg** [Ncm^2]	**Error**
0.035" Glidewire	27	1.9144	2.2252	2.1051	2.0816	5.3535
0.035" Glidewire	28	1.9197	2.2588	2.1926	2.1237	6.4038
0.035" Glidewire	33	2.0070	2.1227	2.1508	2.0935	2.7531
0.035" Glidewire	38	2.4923	2.1416	2.0761	2.2367	7.6196
0.035" Glidewire	43	1.9926	2.2727	2.1376	2.1343	4.4259
0.035" Glidewire	48	2.0463	2.3493	2.1954	2.1970	4.6218
0.035" Glidewire	53	2.0121	2.2864	2.2111	2.1699	4.8461
0.035" Jwire	3	0.1618	0.1666	0.1267	0.1517	10.9885
0.035" Jwire	4	0.1703	0.1596	0.1398	0.1566	7.1238
0.035" Jwire	5	0.1655	0.1577	0.1753	0.1662	3.6503
0.035" Jwire	6	0.2463	0.2475	0.2489	0.2476	0.3525
0.035" Jwire	7	0.3708	0.3750	0.3494	0.3651	2.8643
0.035" Jwire	8	0.5566	0.5501	0.5505	0.5524	0.5056
0.035" Jwire	9	0.7977	0.7586	0.7465	0.7676	2.6133
0.035" Jwire	10	0.9886	0.9561	0.9591	0.9679	1.4224
0.035" Jwire	11	1.1401	1.2130	1.1254	1.1595	3.0756
0.035" Jwire	12	1.3181	1.2794	1.3178	1.3051	1.3121
0.035" Jwire	13	1.4061	1.2873	1.4152	1.3695	4.0059
0.035" Jwire	18	1.4864	1.5468	1.4623	1.4985	2.1479
0.035" Jwire	23	1.4883	1.5151	1.5243	1.5093	0.9244
0.035" Jwire	28	1.5209	1.5009	1.4958	1.5059	0.6638
0.035" Jwire	33	1.4788	1.4726	1.4891	1.4802	0.4024
0.035" Jwire	38	1.5178	1.5096	1.4974	1.5083	0.4777
0.035" Jwire	43	1.4844	1.5167	1.4881	1.4964	0.9051
0.035" Jwire	48	1.5059	1.5309	1.4809	1.5059	1.1066
0.035" Standard Roadrunner	1.5	0.0289	0.0309	0.0357	0.0319	7.9942
0.035" Standard Roadrunner	2.5	0.0289	0.0331	0.0333	0.0318	5.9921
0.035" Standard Roadrunner	3.5	0.0419	0.0534	0.0584	0.0512	12.1900
0.035" Standard Roadrunner	4.5	0.0557	0.0578	0.0575	0.0570	1.5066
0.035" Standard Roadrunner	5.5	0.0886	0.0789	0.0774	0.0816	5.6867
0.035" Standard Roadrunner	6.5	0.1033	0.1035	0.1041	0.1036	0.3194
0.035" Standard Roadrunner	7.5	0.1452	0.1490	0.1467	0.1470	0.9190
0.035" Standard Roadrunner	8.5	0.1902	0.1880	0.1919	0.1900	0.7255
0.035" Standard Roadrunner	9.5	0.2346	0.2343	0.2358	0.2349	0.2596
0.035" Standard Roadrunner	10.5	0.2816	0.2914	0.2834	0.2855	1.3907
0.035" Standard Roadrunner	11.5	0.3625	0.3799	0.3718	0.3714	1.5893
0.035" Standard Roadrunner	12.5	0.5029	0.4844	0.5051	0.4975	1.7523
0.035" Standard Roadrunner	13.5	0.6540	0.6575	0.6716	0.6610	1.0626
0.035" Standard Roadrunner	14.5	0.8199	0.8156	0.8248	0.8201	0.3838
0.035" Standard Roadrunner	15.5	0.8478	0.8536	0.8711	0.8575	1.0542
0.035" Standard Roadrunner	16.5	0.8511	0.8477	0.8521	0.8503	0.2038
0.035" Standard Roadrunner	17.5	0.8596	0.8559	0.8683	0.8613	0.5451
0.035" Standard Roadrunner	18.5	0.8704	0.8657	0.8746	0.8702	0.3485
0.035" Standard Roadrunner	19.5	0.8696	0.8642	0.8797	0.8712	0.6562
0.035" Standard Roadrunner	20.5	0.8753	0.8762	0.8819	0.8778	0.3102
0.035" Standard Roadrunner	21.5	0.8889	0.8763	0.8843	0.8832	0.5181
0.035" Standard Roadrunner	26.5	0.9006	0.8952	0.9033	0.8997	0.3347
0.035" Standard Roadrunner	31.5	0.9048	0.8986	0.9115	0.9050	0.4787
0.035" Standard Roadrunner	36.5	0.9113	0.9080	0.9150	0.9114	0.2609
0.035" Standard Roadrunner	41.5	0.9151	0.9146	0.9119	0.9139	0.1436
0.035" Standard Roadrunner	46.5	0.9136	0.9089	0.9144	0.9123	0.2458
0.035" Stiff Amplatz	2	0.0502	0.0570	0.0678	0.0583	10.8378
0.035" Stiff Amplatz	3	0.0737	0.0822	0.0940	0.0833	8.5511
0.035" Stiff Amplatz	4	0.1477	0.1307	0.1563	0.1449	6.5184
0.035" Stiff Amplatz	5	0.3257	0.3237	0.3367	0.3287	1.6260
0.035" Stiff Amplatz	6	0.5472	0.5439	0.5475	0.5462	0.2768
0.035" Stiff Amplatz	7	0.8994	0.9066	0.8527	0.8862	2.5196
0.035" Stiff Amplatz	8	1.3440	1.3483	1.3085	1.3336	1.2557
0.035" Stiff Amplatz	9	1.9684	1.9934	2.0488	2.0035	1.5055
0.035" Stiff Amplatz	10	2.7715	2.7875	2.7294	2.7628	0.8050
0.035" Stiff Amplatz	11	3.3787	3.3509	3.4704	3.4000	1.3806
0.035" Stiff Amplatz	12	4.1137	4.1635	4.1756	4.1509	0.5978
0.035" Stiff Amplatz	13	7.3114	7.3676	7.1020	7.2604	1.4538
0.035" Stiff Amplatz	14	5.0501	5.1840	5.1130	5.1157	0.8899
0.035" Stiff Amplatz	15	4.8672	5.3461	5.0475	5.0869	3.3964
Continued on next page						

Continuation of Table A.1, Flexural Rigidity Values of All Devices						
Device	**x Position** [cm]	**Test 1** [Ncm^2]	**Test 2** [Ncm^2]	**Test 3** [Ncm^2]	**Avg** [Ncm^2]	**Error**
0.035" Stiff Amplatz	16	5.0570	5.2183	5.1782	5.1512	1.2187
0.035" Stiff Amplatz	17	5.0746	5.3237	5.1227	5.1737	1.9331
0.035" Stiff Amplatz	18	5.3811	5.1907	5.3811	5.3176	1.5910
0.035" Stiff Amplatz	19	5.1577	5.1803	5.2654	5.2011	0.8242
0.035" Stiff Amplatz	20	5.2806	5.5073	5.1775	5.3218	2.3233
0.035" Stiff Amplatz	21	5.4290	5.4159	5.2193	5.3548	1.6860
0.035" Stiff Amplatz	22	5.3241	5.4314	5.2520	5.3359	1.1944
0.035" Stiff Amplatz	23	5.2710	5.3060	5.3471	5.3080	0.4903
0.035" Stiff Amplatz	24	5.2662	5.2511	5.2738	5.2637	0.1600
0.035" Stiff Amplatz	25	5.1320	5.2283	5.2437	5.2013	0.8888
0.035" Stiff Amplatz	30	4.9728	5.0512	5.0602	5.0281	0.7328
0.035" Stiff Amplatz	35	4.9557	5.0469	4.9939	4.9988	0.6412
0.035" Stiff Amplatz	40	5.1051	5.1577	5.0136	5.0921	1.0284
0.035" Stiff Amplatz	45	5.1354	5.1346	5.0062	5.0921	1.1246
0.035" Stiff Amplatz	50	5.0733	5.1633	5.1232	5.1200	0.6069
0.035" Stiff Glidewire	4	0.1034	0.1053	0.1041	0.1042	0.6536
0.035" Stiff Glidewire	5	0.1554	0.1515	0.1512	0.1527	1.1756
0.035" Stiff Glidewire	6	0.2277	0.2166	0.2159	0.2201	2.3230
0.035" Stiff Glidewire	7	0.3189	0.3135	0.2984	0.3102	2.5508
0.035" Stiff Glidewire	8	0.4604	0.4522	0.4308	0.4478	2.5307
0.035" Stiff Glidewire	9	0.6514	0.6305	0.6299	0.6373	1.4796
0.035" Stiff Glidewire	10	0.8512	0.8723	0.8413	0.8549	1.3550
0.035" Stiff Glidewire	11	1.1522	1.1499	1.1196	1.1406	1.2254
0.035" Stiff Glidewire	12	1.5089	1.5198	1.4740	1.5009	1.1946
0.035" Stiff Glidewire	13	1.9453	1.9172	1.8759	1.9128	1.2866
0.035" Stiff Glidewire	14	2.3397	2.3615	2.3304	2.3439	0.5014
0.035" Stiff Glidewire	15	2.8378	2.7911	2.7804	2.8031	0.8251
0.035" Stiff Glidewire	16	3.4512	3.4313	3.4506	3.4444	0.2528
0.035" Stiff Glidewire	17	4.1552	4.0894	4.0594	4.1013	0.8762
0.035" Stiff Glidewire	18	4.9150	4.8147	4.8483	4.8593	0.7636
0.035" Stiff Glidewire	19	5.6805	5.6449	5.5754	5.6336	0.6893
0.035" Stiff Glidewire	20	6.9066	6.6925	6.5622	6.7204	1.8471
0.035" Stiff Glidewire	21	7.3357	7.3328	7.1252	7.2646	1.2789
0.035" Stiff Glidewire	22	7.5712	7.1715	7.1094	7.2840	2.6282
0.035" Stiff Glidewire	23	7.2715	7.3908	7.1869	7.2831	0.9862
0.035" Stiff Glidewire	24	7.3964	7.1590	7.1902	7.2485	1.3598
0.035" Stiff Glidewire	25	7.3107	7.3072	7.4996	7.3725	1.1490
0.035" Stiff Glidewire	26	7.3461	7.1579	7.1389	7.2143	1.2177
0.035" Stiff Glidewire	27	7.3264	7.1349	7.3931	7.2848	1.3716
0.035" Stiff Glidewire	28	7.3397	7.0983	7.1592	7.1991	1.3026
0.035" Stiff Glidewire	29	7.5969	7.1389	7.3134	7.3497	2.2417
0.035" Stiff Glidewire	34	7.3777	7.6457	7.6228	7.5488	1.5102
0.035" Stiff Glidewire	39	7.5253	7.4113	7.2470	7.3945	1.3299
0.035" Stiff Glidewire	44	7.9844	7.5467	7.5276	7.6862	2.5858
0.035" Stiff Glidewire	49	7.8705	7.7102	7.7613	7.7806	0.7698
0.035" Stiff Glidewire	54	7.6423	7.6987	7.6601	7.6671	0.2751
0.035" Stiff Roadrunner	2.5	0.0721	0.0738	0.0748	0.0736	1.3349
0.035" Stiff Roadrunner	3.5	0.0877	0.0918	0.0925	0.0907	2.1722
0.035" Stiff Roadrunner	4.5	0.1305	0.1338	0.1402	0.1348	2.6620
0.035" Stiff Roadrunner	5.5	0.1984	0.2025	0.2084	0.2031	1.7406
0.035" Stiff Roadrunner	6.5	0.3065	0.3038	0.2968	0.3024	1.2319
0.035" Stiff Roadrunner	7.5	0.4607	0.4558	0.4938	0.4701	3.3633
0.035" Stiff Roadrunner	8.5	0.6425	0.6402	0.6835	0.6554	2.8593
0.035" Stiff Roadrunner	9.5	0.8671	0.8753	0.9106	0.8843	1.9816
0.035" Stiff Roadrunner	10.5	1.1560	1.1632	1.1461	1.1551	0.5220
0.035" Stiff Roadrunner	11.5	1.5166	1.5060	1.5132	1.5119	0.2607
0.035" Stiff Roadrunner	12.5	1.9118	1.9064	1.9067	1.9083	0.1225
0.035" Stiff Roadrunner	13.5	2.3518	2.3879	2.3646	2.3681	0.5559
0.035" Stiff Roadrunner	14.5	2.8916	2.9065	2.8910	2.8964	0.2338
0.035" Stiff Roadrunner	15.5	3.3428	3.3472	3.3398	3.3432	0.0785
0.035" Stiff Roadrunner	16.5	3.5759	3.5673	3.6297	3.5910	0.7194
0.035" Stiff Roadrunner	17.5	3.8637	3.9120	3.9263	3.9007	0.6312
0.035" Stiff Roadrunner	18.5	4.6937	4.6813	4.6858	4.6869	0.0964
0.035" Stiff Roadrunner	19.5	6.2222	6.3038	6.1574	6.2278	0.8131
0.035" Stiff Roadrunner	20.5	7.3626	7.4118	7.2976	7.3573	0.5410
Continued on next page						

Continuation of Table A.1, Flexural Rigidity Values of All Devices					
Device	x Position [cm]	Test 1 [Ncm^2]	Test 2 [Ncm^2]	Test 3 [Ncm^2]	Avg [Ncm^2]	Error
0.035" Stiff Roadrunner	21.5	7.6280	7.5805	7.5819	7.5968	0.2736
0.035" Stiff Roadrunner	26.5	7.9574	7.6556	7.7922	7.8017	1.3304
0.035" Stiff Roadrunner	31.5	7.8899	7.7398	7.7993	7.8097	0.6851
0.035" Stiff Roadrunner	36.5	7.8731	7.8021	7.8821	7.8524	0.4275
0.035" Stiff Roadrunner	41.5	7.8865	7.8887	7.9574	7.9108	0.3924
0.035" Stiff Roadrunner	46.5	7.8788	7.9350	7.9434	7.9191	0.3393
0.071" Benchmark	2	0.2697	0.2713	0.2896	0.2769	3.0589
0.071" Benchmark	3	0.2955	0.2926	0.2960	0.2947	0.4664
0.071" Benchmark	4	0.4688	0.4692	0.4958	0.4779	2.4892
0.071" Benchmark	5	0.5468	0.5615	0.5436	0.5506	1.3158
0.071" Benchmark	6	0.6330	0.6461	0.6296	0.6362	1.0376
0.071" Benchmark	7	0.9334	0.8570	0.9234	0.9046	3.5078
0.071" Benchmark	8	1.2383	1.2952	1.2801	1.2712	1.7273
0.071" Benchmark	9	1.7057	1.7173	1.7373	1.7201	0.6683
0.071" Benchmark	10	1.9857	2.0131	2.1050	2.0346	2.3060
0.071" Benchmark	11	2.0718	2.2115	2.1939	2.1591	2.6935
0.071" Benchmark	12	2.7130	2.5882	2.9743	2.7585	5.2153
0.071" Benchmark	13	3.8824	3.9703	3.9453	3.9327	0.8516
0.071" Benchmark	14	4.4873	4.3784	4.4927	4.4528	1.1138
0.071" Benchmark	15	7.2207	6.8630	6.7238	6.9358	2.7380
0.071" Benchmark	16	6.6230	6.4539	6.5374	6.5381	0.8657
0.071" Benchmark	17	6.4658	6.4460	6.5901	6.5007	0.9175
0.071" Benchmark	18	7.0858	6.6486	6.7490	6.8278	2.5190
0.071" Benchmark	19	6.5923	7.0399	6.5642	6.7322	3.0478
0.071" Benchmark	20	6.6293	6.7338	6.6848	6.6826	0.5324
0.071" Benchmark	25	6.5329	6.4320	6.3798	6.4482	0.8755
0.071" Benchmark	30	6.7835	7.3514	6.9208	7.0186	3.1613
0.071" Benchmark	35	6.7287	6.5536	6.5184	6.6002	1.2974
0.071" Benchmark	40	7.1172	6.8837	6.8164	6.9391	1.7107
0.071" Rist	1.5	0.2627	0.2659	0.2720	0.2669	1.2854
0.071" Rist	2.5	0.2508	0.2667	0.2839	0.2672	4.1817
0.071" Rist	3.5	0.2889	0.2838	0.3459	0.3062	8.6408
0.071" Rist	4.5	0.4508	0.4148	0.4174	0.4276	3.6041
0.071" Rist	5.5	0.4946	0.4742	0.4766	0.4818	1.7757
0.071" Rist	6.5	0.5903	0.5645	0.5770	0.5773	1.5009
0.071" Rist	7.5	0.9650	0.9831	0.9650	0.9710	0.8312
0.071" Rist	8.5	0.9496	1.0040	0.9841	0.9792	2.0168
0.071" Rist	9.5	0.9321	0.9725	1.0186	0.9744	3.0215
0.071" Rist	10.5	1.4275	1.3845	1.3626	1.3915	1.7217
0.071" Rist	11.5	1.8443	1.7591	1.8053	1.8029	1.6189
0.071" Rist	12.5	1.9200	1.9476	1.8848	1.9175	1.1345
0.071" Rist	13.5	1.7926	1.8139	1.7475	1.7846	1.3880
0.071" Rist	14.5	1.9530	1.9024	2.1201	1.9918	4.2931
0.071" Rist	15.5	2.5884	2.5764	2.5486	2.5711	0.5838
0.071" Rist	16.5	4.9137	4.5413	4.3243	4.5931	4.6532
0.071" Rist	17.5	5.0048	5.0745	4.9735	5.0176	0.7560
0.071" Rist	18.5	5.8103	5.6903	5.6449	5.7151	1.1097
0.071" Rist	19.5	6.4657	6.5730	6.2146	6.4177	2.1104
0.071" Rist	20.5	6.7361	6.6458	6.5490	6.6436	0.9495
0.071" Rist	21.5	6.2365	6.0796	6.1289	6.1483	0.9560
0.071" Rist	22.5	5.8225	5.9130	5.8242	5.8532	0.6801
0.071" Rist	23.5	6.0093	6.0920	5.8824	5.9946	1.2471
0.071" Rist	24.5	6.3831	6.1978	6.0693	6.2167	1.7840
0.071" Rist	25.5	6.1084	5.9602	6.3060	6.1249	1.9712
0.071" Rist	26.5	6.1790	5.9414	5.9535	6.0246	1.7085
0.071" Rist	27.5	6.4602	6.1159	5.9601	6.1787	3.0370
0.071" Rist	28.5	6.5510	6.2396	6.0726	6.2877	2.7914
0.071" Rist	29.5	6.3106	6.1884	6.2224	6.2404	0.7491
0.071" Rist	30.5	6.0485	6.0383	6.2914	6.1260	1.7993
0.071" Rist	31.5	5.9666	6.1508	5.8348	5.9841	1.8576
0.071" Rist	36.5	6.3406	6.2675	6.2734	6.2938	0.4950
0.071" Rist	41.5	6.3879	6.7626	6.4094	6.5200	2.4806
0.079" Rist	2	0.3416	0.3529	0.3607	0.3517	1.9269
0.079" Rist	3	0.3554	0.3557	0.3550	0.3554	0.0677
0.079" Rist	4	0.4974	0.4818	0.4745	0.4846	1.7614
Continued on next page					

[25]

Continuation of Table A.1, Flexural Rigidity Values of All Devices						
Device	x Position $[cm]$	Test 1 $[Ncm^2]$	Test 2 $[Ncm^2]$	Test 3 $[Ncm^2]$	Avg $[Ncm^2]$	Error
0.079" Rist	5	0.6364	0.6362	0.6409	0.6378	0.3172
0.079" Rist	6	0.6930	0.7011	0.6866	0.6936	0.7234
0.079" Rist	7	0.8787	0.9371	0.8896	0.9018	2.6070
0.079" Rist	8	1.0149	1.0527	1.0824	1.0500	2.2312
0.079" Rist	9	1.2363	1.2193	1.2416	1.2324	0.7094
0.079" Rist	10	1.5346	1.5093	1.5018	1.5152	0.8512
0.079" Rist	11	1.5697	1.5900	1.5571	1.5722	0.7525
0.079" Rist	12	1.5771	1.6848	1.6940	1.6520	3.0228
0.079" Rist	13	1.9801	2.0750	1.9817	2.0122	2.0784
0.079" Rist	14	2.6089	2.8449	2.9646	2.8062	4.6854
0.079" Rist	15	2.1322	2.3243	2.6525	2.3696	7.9572
0.079" Rist	16	2.1292	2.2779	2.4373	2.2815	4.5521
0.079" Rist	17	2.3254	2.3539	2.7052	2.4615	6.5999
0.079" Rist	18	2.6444	2.6929	2.7660	2.7011	1.6016
0.079" Rist	19	3.2717	3.4956	3.5949	3.4541	3.5194
0.079" Rist	20	3.7174	3.6996	4.2027	3.8732	5.6709
0.079" Rist	21	3.8819	3.9843	4.1309	3.9991	2.1982
0.079" Rist	22	3.8448	4.0300	4.1274	4.0007	2.5983
0.079" Rist	23	4.2101	4.1981	4.2581	4.2221	0.5686
0.079" Rist	24	5.5342	5.3647	5.8060	5.5683	2.8456
0.079" Rist	25	6.2534	6.3931	6.4703	6.3723	1.2433
0.079" Rist	26	6.1515	6.3999	6.4823	6.3446	2.0286
0.079" Rist	27	6.3845	5.9867	6.3232	6.2315	2.6188
0.079" Rist	28	6.2743	6.3478	6.2053	6.2758	0.7649
0.079" Rist	29	6.8399	7.0578	6.7995	6.8991	1.5335
0.079" Rist	30	7.8534	8.0677	8.1363	8.0191	1.3781
0.079" Rist	35	8.2643	8.4365	8.4103	8.3704	0.8449
0.079" Rist	40	8.6385	8.4530	8.6081	8.5665	0.8835
0.088" Ballast	1.5	1.8352	1.8514	1.7383	1.8083	2.5802
0.088" Ballast	2.5	1.9406	1.9248	1.9338	1.9330	0.2839
0.088" Ballast	3.5	1.9915	1.9685	2.0114	1.9905	0.7360
0.088" Ballast	4.5	1.9647	2.1008	2.1422	2.0692	3.3682
0.088" Ballast	5.5	2.3460	2.3488	2.3434	2.3461	0.0786
0.088" Ballast	6.5	3.0083	2.9310	2.8921	2.9438	1.4609
0.088" Ballast	7.5	3.4396	3.7796	3.7202	3.6465	3.7818
0.088" Ballast	8.5	5.5717	5.6361	5.8146	5.6741	1.6502
0.088" Ballast	9.5	6.6116	6.5601	6.3208	6.4975	1.8126
0.088" Ballast	10.5	8.0976	9.2387	9.3482	8.8948	5.9751
0.088" Ballast	11.5	8.3650	8.0339	8.6168	8.3385	2.4354
0.088" Ballast	12.5	9.9368	11.0073	10.3676	10.4372	3.6416
0.088" Ballast	13.5	10.3189	10.2553	12.0253	10.8665	7.1092
0.088" Ballast	14.5	15.5870	13.5701	14.6479	14.6017	4.7098
0.088" Ballast	15.5	17.3899	18.6374	18.1168	18.0480	2.4311
0.088" Ballast	16.5	17.1337	19.4325	19.2198	18.5953	5.2402
0.088" Ballast	17.5	19.5892	19.7693	19.2031	19.5206	1.0841
0.088" Ballast	18.5	19.4657	17.9503	18.3068	18.5743	3.1994
0.088" Ballast	19.5	19.2169	18.8719	20.3883	19.4924	3.0643
0.088" Ballast	20.5	20.2032	20.1289	19.9385	20.0902	0.5033
0.088" Ballast	26.5	18.5895	18.0043	17.8154	18.1364	1.6655
0.088" Ballast	31.5	19.0615	19.2574	19.0538	19.1242	0.4642
0.088" Ballast	36.5	18.1188	17.5977	17.6002	17.7722	1.2999
0.088" Ballast	41.5	17.0986	16.9284	16.9590	16.9953	0.4052
0.088" Neuron Max	2	1.6082	1.9637	1.8881	1.8200	7.7586
0.088" Neuron Max	3	2.5940	2.5669	2.5489	2.5699	0.6237
0.088" Neuron Max	4	2.8971	2.7656	2.8323	2.8317	1.5559
0.088" Neuron Max	5	3.5466	3.4275	3.3727	3.4489	1.8885
0.088" Neuron Max	6	4.0591	3.9485	3.8865	3.9647	1.5868
0.088" Neuron Max	7	5.0366	5.2094	5.0233	5.0898	1.5664
0.088" Neuron Max	8	6.4916	6.7673	6.5611	6.6067	1.6212
0.088" Neuron Max	9	8.1169	8.1250	8.0915	8.1112	0.1612
0.088" Neuron Max	10	9.7471	9.8729	9.7766	9.7989	0.5036
0.088" Neuron Max	11	10.9327	10.9977	11.0405	10.9903	0.3494
0.088" Neuron Max	12	12.1094	12.2857	12.1654	12.1868	0.5408
0.088" Neuron Max	13	12.5327	12.7412	12.7025	12.6588	0.6641
0.088" Neuron Max	18	15.7240	16.1675	16.1804	16.0239	1.2480
Continued on next page						

[26]

Continuation of Table A.1, Flexural Rigidity Values of All Devices					
Device	**x Position** $[cm]$	**Test 1** $[Ncm^2]$	**Test 2** $[Ncm^2]$	**Test 3** $[Ncm^2]$	**Avg** $[Ncm^2]$	**Error**
0.088" Neuron Max	23	15.6848	16.5382	16.3601	16.1944	2.0976
0.088" Neuron Max	28	15.9804	15.8588	16.0732	15.9708	0.4674
0.088" Neuron Max	33	15.8624	16.3070	16.1750	16.1148	1.0443
0.088" Neuron Max	38	15.1890	14.8793	14.4271	14.8318	1.8190
0.088" Neuron Max	43	16.2830	15.8489	16.4113	16.1811	1.3686
6F Flexor Shuttle	1.5	2.0757	1.7152	1.8619	1.8843	6.7723
6F Flexor Shuttle	2.5	2.0567	1.8162	1.9057	1.9262	4.5164
6F Flexor Shuttle	3.5	1.8841	1.8288	1.8657	1.8595	1.1026
6F Flexor Shuttle	4.5	1.7489	1.7188	1.7733	1.7470	1.0763
6F Flexor Shuttle	5.5	1.7371	1.7561	1.8854	1.7929	3.4415
6F Flexor Shuttle	6.5	1.9774	1.8254	1.8858	1.8962	2.8535
6F Flexor Shuttle	7.5	2.7153	2.3679	2.5023	2.5285	4.9252
6F Flexor Shuttle	8.5	4.1534	4.0151	4.0927	4.0871	1.1740
6F Flexor Shuttle	9.5	4.2966	4.0927	4.0494	4.1463	2.4180
6F Flexor Shuttle	10.5	4.3133	3.9188	3.9781	4.0701	3.9836
6F Flexor Shuttle	11.5	4.2497	4.0353	4.0595	4.1148	2.1850
6F Flexor Shuttle	16.5	4.2009	4.0543	4.1292	4.1281	1.1920
6F Flexor Shuttle	21.5	4.1369	4.0632	4.2030	4.1344	1.1471
6F Flexor Shuttle	26.5	4.3732	4.3576	4.2910	4.3406	0.7615
6F Flexor Shuttle	31.5	4.3995	4.5432	4.5571	4.5000	1.4885
6F Flexor Shuttle	36.5	4.7570	4.7702	4.5936	4.7069	1.6050
6F Flexor Shuttle	41.5	4.8243	4.7996	4.6249	4.7496	1.7506
6F SOFIA	1.5	0.0786	0.0721	0.0765	0.0758	3.1990
6F SOFIA	2.5	0.1371	0.1321	0.1300	0.1330	2.0054
6F SOFIA	3.5	0.1621	0.1585	0.1531	0.1579	2.0178
6F SOFIA	4.5	0.1872	0.1870	0.1825	0.1856	1.0974
6F SOFIA	5.5	0.2063	0.1974	0.1966	0.2001	2.0754
6F SOFIA	6.5	0.2029	0.1886	0.1842	0.1919	3.8210
6F SOFIA	7.5	0.2546	0.2496	0.2315	0.2452	3.7456
6F SOFIA	8.5	0.2548	0.2523	0.2292	0.2455	4.4131
6F SOFIA	9.5	0.2187	0.2091	0.2041	0.2106	2.5514
6F SOFIA	10.5	0.2696	0.2603	0.2447	0.2582	3.4840
6F SOFIA	11.5	0.2323	0.2233	0.2323	0.2293	1.7459
6F SOFIA	12.5	0.2265	0.2217	0.2253	0.2245	0.8245
6F SOFIA	13.5	0.2869	0.2751	0.2697	0.2772	2.3248
6F SOFIA	14.5	0.3076	0.3008	0.2950	0.3011	1.4254
6F SOFIA	15.5	0.4062	0.3903	0.3958	0.3974	1.4692
6F SOFIA	16.5	0.8738	0.7651	0.8096	0.8162	4.7088
6F SOFIA	17.5	1.1724	1.1136	1.1320	1.1394	1.9348
6F SOFIA	18.5	1.2793	1.1780	1.2466	1.2346	3.0585
6F SOFIA	19.5	1.8409	1.8846	1.7804	1.8353	1.9945
6F SOFIA	20.5	1.7003	1.7267	1.7518	1.7263	1.0033
6F SOFIA	21.5	2.0249	2.0362	1.9534	2.0048	1.7106
6F SOFIA	22.5	2.5518	2.4986	2.4991	2.5165	0.9350
6F SOFIA	23.5	2.5887	2.6429	2.5793	2.6037	1.0050
6F SOFIA	24.5	2.7272	2.6162	2.6260	2.6565	1.7747
6F SOFIA	25.5	2.6224	2.5999	2.6142	2.6122	0.3140
6F SOFIA	26.5	2.9921	2.8862	2.8926	2.9236	1.5609
6F SOFIA	27.5	3.0165	2.9996	3.0296	3.0152	0.3453
6F SOFIA	28.5	3.9219	3.8511	3.7973	3.8568	1.1261
6F SOFIA	29.5	4.1424	4.0462	4.1517	4.1134	1.0893
6F SOFIA	30.5	4.1944	4.1206	4.0879	4.1343	0.9698
6F SOFIA	31.5	5.7570	5.5180	5.5536	5.6095	1.7521
6F SOFIA	32.5	5.7291	5.6279	5.8658	5.7409	1.4498
6F SOFIA	33.5	7.4900	7.1728	7.2273	7.2967	1.7660
6F SOFIA	34.5	7.6759	7.6333	7.3497	7.5530	1.7945
6F SOFIA	35.5	7.7690	7.4422	7.7342	7.6485	1.7980
6F SOFIA	40.5	7.7443	7.4602	7.4274	7.5439	1.7705
AXS Catalyst 5	1.5	0.2339	0.2333	0.2478	0.2383	2.6487
AXS Catalyst 5	2.5	0.2312	0.2467	0.2431	0.2404	2.5363
AXS Catalyst 5	3.5	0.3519	0.3001	0.3116	0.3212	6.3694
AXS Catalyst 5	4.5	0.3435	0.3399	0.3281	0.3372	1.7961
AXS Catalyst 5	5.5	0.5030	0.5441	0.5357	0.5276	3.1054
AXS Catalyst 5	6.5	0.5655	0.6235	0.6133	0.6008	3.9108
AXS Catalyst 5	7.5	0.5804	0.5959	0.6038	0.5934	1.4578
Continued on next page					

Continuation of Table A.1, Flexural Rigidity Values of All Devices						
Device	**x Position** $[cm]$	**Test 1** $[Ncm^2]$	**Test 2** $[Ncm^2]$	**Test 3** $[Ncm^2]$	**Avg** $[Ncm^2]$	**Error**
AXS Catalyst 5	8.5	0.6280	0.6239	0.6021	0.6180	1.7161
AXS Catalyst 5	9.5	0.6230	0.6160	0.6121	0.6171	0.6454
AXS Catalyst 5	10.5	0.6459	0.5977	0.6184	0.6206	2.7135
AXS Catalyst 5	11.5	0.9666	0.9613	0.9699	0.9660	0.3179
AXS Catalyst 5	12.5	1.0342	1.0355	1.0617	1.0438	1.1413
AXS Catalyst 5	13.5	1.0602	1.0893	1.0749	1.0748	0.9068
AXS Catalyst 5	14.5	1.0375	1.0897	1.0198	1.0490	2.5877
AXS Catalyst 5	15.5	1.1031	1.1626	1.1400	1.1352	1.8859
AXS Catalyst 5	16.5	1.1724	1.1702	1.1615	1.1680	0.3738
AXS Catalyst 5	17.5	1.3399	1.3188	1.2906	1.3164	1.3103
AXS Catalyst 5	18.5	1.5780	1.6049	1.5835	1.5888	0.6741
AXS Catalyst 5	19.5	1.6232	1.5932	1.5882	1.6015	0.9009
AXS Catalyst 5	20.5	1.7439	1.7886	1.6944	1.7423	1.8335
AXS Catalyst 5	21.5	1.7072	1.7230	1.7143	1.7148	0.3162
AXS Catalyst 5	22.5	1.7172	1.7024	1.7081	1.7092	0.3110
AXS Catalyst 5	23.5	1.7027	1.7770	1.7304	1.7367	1.5487
AXS Catalyst 5	24.5	1.8063	1.9432	1.9078	1.8858	2.8091
AXS Catalyst 5	25.5	2.6213	2.6734	2.6502	2.6483	0.6787
AXS Catalyst 5	26.5	2.6497	2.7207	2.7176	2.6960	1.1447
AXS Catalyst 5	27.5	2.6853	2.7692	2.7559	2.7368	1.2546
AXS Catalyst 5	28.5	2.7295	2.8592	2.7927	2.7938	1.5601
AXS Catalyst 5	29.5	2.7950	2.9405	2.9045	2.8800	1.9669
AXS Catalyst 5	30.5	2.8933	2.9335	2.8453	2.8907	1.0477
AXS Catalyst 5	31.5	3.3498	3.4215	3.3096	3.3603	1.2141
AXS Catalyst 5	32.5	4.2208	4.3753	4.3182	4.3048	1.3005
AXS Catalyst 5	33.5	4.3177	4.3784	4.2906	4.3289	0.7627
AXS Catalyst 5	34.5	4.4504	4.5175	4.5051	4.4910	0.6029
AXS Catalyst 5	35.5	4.4183	4.6290	4.5645	4.5373	1.7480
AXS Catalyst 5	36.5	4.1969	4.3686	4.3653	4.3103	1.7540
AXS Catalyst 5	37.5	3.8804	3.9257	3.9637	3.9233	0.7276
AXS Catalyst 5	38.5	4.0555	4.0270	4.0497	4.0441	0.2822
AXS Catalyst 5	39.5	4.0477	3.9337	3.9897	3.9904	0.9582
AXS Catalyst 5	40.5	3.8929	3.9008	3.9013	3.8983	0.0924
AXS Catalyst 5	41.5	5.2275	5.2316	5.1985	5.2192	0.2645
AXS Catalyst 5	46.5	5.2878	5.2732	5.3614	5.3075	0.6774
AXS Infinity	1.5	2.2038	2.1825	2.2062	2.1975	0.4558
AXS Infinity	2.5	2.2034	2.2228	2.2377	2.2213	0.5366
AXS Infinity	3.5	2.2565	2.2760	2.2740	2.2688	0.3628
AXS Infinity	4.5	2.8267	2.9096	2.8576	2.8646	1.0464
AXS Infinity	5.5	5.2839	5.3444	5.2949	5.3077	0.4611
AXS Infinity	6.5	5.4907	5.4996	5.4296	5.4733	0.5321
AXS Infinity	7.5	6.4946	6.4675	6.1911	6.3844	2.0186
AXS Infinity	8.5	7.5021	7.5053	7.4103	7.4726	0.5558
AXS Infinity	9.5	10.0873	10.1548	10.5224	10.2548	1.7394
AXS Infinity	10.5	15.4050	14.9932	15.0000	15.1327	1.1995
AXS Infinity	11.5	15.3429	14.9860	15.1351	15.1547	0.8282
AXS Infinity	12.5	15.3840	15.0613	15.0034	15.1495	1.0318
AXS Infinity	13.5	15.3124	15.1831	15.1423	15.2126	0.4373
AXS Infinity	14.5	15.5528	15.4873	15.3887	15.4763	0.3773
AXS Infinity	15.5	15.5367	15.3016	15.4192	15.4192	0.5082
AXS Infinity	16.5	15.5578	15.4055	15.3524	15.4385	0.5148
AXS Infinity	21.5	15.2585	15.4160	15.3788	15.3511	0.4021
AXS Infinity	26.5	16.0931	15.3451	15.1425	15.5269	2.4310
AXS Infinity	31.5	16.0234	15.3062	15.3507	15.5601	1.9850
AXS Infinity	36.5	15.5166	16.1101	15.5444	15.7237	1.6383
AXS Infinity	41.5	15.7772	15.5594	15.5949	15.6438	0.5682
Zoom 88	1.5	0.2231	0.1992	0.1976	0.2066	5.3245
Zoom 88	2.5	0.2587	0.2480	0.2375	0.2481	2.8524
Zoom 88	3.5	0.4321	0.4444	0.4284	0.4350	1.4469
Zoom 88	4.5	0.4282	0.4652	0.4497	0.4477	2.9084
Zoom 88	5.5	0.4439	0.4969	0.5069	0.4826	5.3369
Zoom 88	6.5	0.4647	0.5556	0.5451	0.5218	7.2904
Zoom 88	7.5	0.5365	0.5776	0.5671	0.5604	2.8452
Zoom 88	8.5	0.5428	0.6160	0.7180	0.6256	9.8476
Zoom 88	9.5	0.7014	0.7417	0.6529	0.6987	4.3661
Continued on next page						

[28]

	Continuation of Table A.1, Flexural Rigidity Values of All Devices					
Device	**x Position** $[cm]$	**Test 1** $[Ncm^2]$	**Test 2** $[Ncm^2]$	**Test 3** $[Ncm^2]$	**Avg** $[Ncm^2]$	**Error**
Zoom 88	10.5	1.0085	0.9880	1.0758	1.0241	3.3675
Zoom 88	11.5	1.3813	1.4625	1.5147	1.4528	3.2827
Zoom 88	12.5	1.8068	1.8613	1.8652	1.8444	1.3606
Zoom 88	13.5	2.4554	2.8183	2.6189	2.6309	4.7496
Zoom 88	14.5	3.2966	3.3515	3.5177	3.3886	2.5400
Zoom 88	15.5	4.9271	4.6583	4.8645	4.8166	2.1918
Zoom 88	16.5	6.3153	6.0665	6.1158	6.1659	1.6159
Zoom 88	17.5	7.2559	7.3553	7.2221	7.2778	0.7102
Zoom 88	18.5	8.1535	8.1310	8.0686	8.1177	0.4030
Zoom 88	19.5	8.3113	8.0839	8.3793	8.2582	1.4071
Zoom 88	24.5	6.1112	6.3983	6.8338	6.4478	3.9915
Zoom 88	29.5	7.3524	7.4418	7.6486	7.4809	1.4940
Zoom 88	34.5	6.8701	6.8511	6.7615	6.8276	0.6454
Zoom 88	39.5	6.6087	6.5573	6.5326	6.5662	0.4315

Appendix B

MATLAB Code

B.1 Flexural Rigidity Calculator

This is an example of the code used to calculate the flexural rigidity values of endovascular devices, in this case calculating the flexural rigidity values of a 0.035" RoadRunner guidewire. This section of code uses the data output by the load cell amplifier, the known test positions, and the known CNC parameters to calculate the flexural rigidity values at each point tested.

```
close all hidden
clear

mm_pix = 0.264;

for k = 1:3
    % ---- %
    test_name = 'roadRunner180_';
    data = readmatrix([test_name,num2str(k)]);
    x = readmatrix('RoadRunnerDistances.xlsx');
    test_points = length(x);
    toggleSave = 0;
    threshold = .2;
    minPeakDist = 150;
    % ---- %

    feed_rate = 0.5;
```

```matlab
test_length = 3;
sampling_rate = 0.1;

data(data > 1) = 0;
data(isnan(data)) = 0;
for i = 2:1:length(data)-1
    if data(i) == 0
        data(i) = (data(i-1)+data(i+1))/2;
    end
end

time = sampling_rate:sampling_rate:sampling_rate*length(data);
time = time';
force = -1*data;

abv_thresh = find(force > threshold);
end_pts = find(diff(abv_thresh) > 1);

ind_start = [abv_thresh(1)-1;abv_thresh(end_pts+1)-1];
ind_stop = [abv_thresh(end_pts)+1;abv_thresh(end)+1];

start_time = time(ind_start);
start_force = force(ind_start);
stop_time = time(ind_stop);
stop_force = force(ind_stop);

[pks, peak_ind] = findpeaks(force,'SortStr','descend','NPeaks', ...
    test_points,'Threshold',0.0001,'MinPeakDistance',minPeakDist);

peak_ind = sort(peak_ind);
peak_time = time(peak_ind);
peak_force = force(peak_ind);

peaksDimensions = [0 0 125 70];
```

```matlab
figure('Position',floor(peaksDimensions./mm_pix))
plot(time,force,'LineWidth',1.5)
hold on
plot(start_time,start_force,'o')
plot(stop_time,stop_force,'o')
plot(peak_time,peak_force,'o')
ylabel('Force [gf]')
xlabel('Time [s]')
set(gca,'FontName','Arial', 'FontSize',8)

EI = zeros(1,test_points);
Rsq = zeros(1,test_points);

lineFit = [80 80 125 70];
figure('Position',floor(lineFit./mm_pix))

dim = [.2 .5 .3 .3];

for i=1:test_points
    fd_time = time(ind_start(i):peak_ind(i));
    fd_force = force(ind_start(i):peak_ind(i));
    fd_time = fd_time-min(fd_time);
    fd_disp = fd_time*feed_rate;

    [fit, S] = polyfit(fd_disp,fd_force,1);
    yfit = polyval(fit,fd_disp);

    SStot = sum((fd_force-mean(fd_force)).^2);
    SSres = sum((fd_force-yfit).^2);
    Rsq(i) = 1-SSres/SStot;

    subplot(2,ceil(test_points/2),i)
    plot(fd_disp,fd_force,'-o');
    hold on
```

[32]

```matlab
        plot(fd_disp,yfit)
        str = ['Point ',num2str(i)];
        str2 = ['R^2=',num2str(Rsq(i))];
        xlabel('Displacement [mm]')
        ylabel('Force [gf]')

        dummyh = line(nan, nan, 'Linestyle', 'none', 'Marker', 'none', ...
            'Color', 'none');
        dummyh2 = line(nan, nan, 'Linestyle', 'none', 'Marker', 'none', ...
            'Color', 'none');
        legend([dummyh, dummyh2], str, str2, 'Location', ...
            'northoutside','FontWeight','bold');
        legend('boxoff')

        EI(i) = (fit(1)*10/1000*9.81)*(test_length^3/48);

        set(gca,'FontName','Arial','FontSize', 8)
    end
    EIall(k,:) = EI;
    ax = gcf;
    if toggleSave == 1
        save([test_name,num2str(k)],'time','data','EI')
    end
end
%%

StackedDimensions = [0 0 125 45];
figure('Position',floor(StackedDimensions./mm_pix))
hold on
for i=1:3
    load([test_name,num2str(i)])
    EI_com = EIall;
    plot(x,EIall(i,:),'- .','MarkerSize',10,'LineWidth',1)
end
```

```matlab
avg = mean(EI_com);
err = std(EI_com);
errorbar(x,avg,err,'- .','LineWidth',1,'MarkerSize',10,'CapSize',12)
xlabel('Distance from distal tip [cm]')
ylabel('Flexural rigidity, [Ncm^2]')
legend('Test 1','Test 2','Test 3','Average','Location','southeast')
ylim([0 10])
set(gca,'FontName','Aral', 'FontSize',8)
ax = gcf;

figure('Position',floor(StackedDimensions./mm_pix))
errorbar(x,avg,err,'- .','LineWidth',1,'MarkerSize',10,'CapSize',10)
xlabel('Distance from distal tip [cm]')
ylabel('Flexural rigidity [Ncm^2]')
ylim([0 10])
set(gca,'FontName','Arial')
ax = gcf;
exportgraphics(ax, strcat(test_name,'_combined.png'), 'Resolution', 300)
save(test_name, "x", "avg", "err")

%%
EIdimensions = [0 0 35 50];
figure('Position',floor(EIdimensions./mm_pix))
plot(fd_disp,fd_force,'o');
hold on
plot(fd_disp,yfit)
xlabel('Displacement [mm]')
ylabel('Force [gf]')
str = ['Point ',num2str(25)];
str2 = ['R^2=',num2str(Rsq(:,25))];
fullstr = [str,newline,str2];
dummyh = line(nan, nan, 'Linestyle', 'none', 'Marker', 'none', 'Color', ...
    'none');
dummyh2 = line(nan, nan, 'Linestyle', 'none', 'Marker', 'none', 'Color' ...
```

```
       , 'none');
annotation('textbox',[.24 .83 .1 .1],'String',fullstr,'EdgeColor', ...
     'none','FontSize',8,'FontName','Arial')
set(gca, 'YLim',[-30 300], 'FontName', 'Arial', 'FontSize', 8)


peaksDimensions = [0 0 70 50];
figure('Position',floor(peaksDimensions./mm_pix))
plot((time-605),force,'LineWidth',1)
hold on
plot(start_time-605,start_force,'o')
plot(stop_time-605,stop_force,'o')
plot(peak_time-605,peak_force,'o')
ylabel('Force [gf]')
xlabel('Time [s]')
set(gca,'FontName','Arial','XLim',[605-605 620-605],'YLim',[0 300], ...
     'FontSize',8)
```

B.2   Struct-Making Code

This portion of code parses through the data from each test and connects each test, its
average, and its error within a sub-struct housed within a larger struct that categorizes by
device type, then device.

```
    clc
clear

fileNames = uigetfile('*.xlsx', 'Select Excel Files', 'MultiSelect', 'on');
selectedFiles = {};

grouping = readtable('DeviceList.xlsx');

for i = 1:length(fileNames)
```

[35]

```matlab
    [~, fileNameWithoutExtension, ~] = fileparts(fileNames{i});
    selectedFiles{i} = fileNameWithoutExtension;
end


structData = struct('wire',[],'longSheath',[],'catheter',[]);


for i = 1:length(selectedFiles)
    data = readmatrix(append(string(selectedFiles(i)), '.xlsx'));
    filename = string(selectedFiles(i));
    name = erase(filename," ");

    if any(strcmp(filename,grouping.Wire))
        temp = struct('x',      data(:,1), ...
                            'test1',  data(:,2), ...
                            'test2',  data(:,3), ...
                            'test3',  data(:,4), ...
                            'Avg',    data(:,5), ...
                            'Err',    data(:,6), ...
                            'Name', filename);
        structData.wire.(strcat('w',name)) = temp;
    end
    if any(strcmp(filename,grouping.LongSheath))
        temp = struct('x',      data(:,1), ...
                            'test1',  data(:,2), ...
                            'test2',  data(:,3), ...
                            'test3',  data(:,4), ...
                            'Avg',    data(:,5), ...
                            'Err',    data(:,6), ...
                            'Name', filename);
        structData.longSheath.(strcat('ls',name)) = temp;
    end
    if any(strcmp(filename,grouping.Catheter))
        temp = struct('x',      data(:,1), ...
                            'test1',  data(:,2), ...
```

```
                    'test2',  data(:,3), ...
                    'test3',  data(:,4), ...
                    'Avg',    data(:,5), ...
                    'Err',    data(:,6), ...
                    'Name', filename);
        structData.catheter.(strcat('c',name)) = temp;
    end
end
```

B.3   Stacked Lengthwise Flexural Rigidity Graphing Code

This section of code uses the struct containing all the devices generated by the code in Appendix B.2 to graph the flexural rigidity values along the length of multiple endovascular devices, grouped by device type.

```
    close all hidden
clear
clc


load('structData.mat')
grouping = readtable('DeviceList.xlsx');
mm_pix = 0.264;
markers = ['o-';'*-';'.-';'x-';'s-';'d-';'^-';'v-';'>-';'<-';'p-'];
markers = [markers; markers];
newColor = {'#78b4c6', '#871d32', '#54c069', '#326f9c', '#a0b460',...
    '#e94c42', '#0b6d33', '#de886a', '#563225'};


%% Wires

wiredims = [0 0 180 90];
figure('Position',floor(wiredims./mm_pix))
```

```matlab
hold on

wirefieldnames = fieldnames(structData.wire);

for i = 1:length(wirefieldnames)

    ind = find(strcmp(wirefieldnames,strcat('w',erase(grouping.Wire(i)...
        ," "))));

    name = wirefieldnames{ind};
    wireLegend(i) = structData.wire.(name).Name;
    errorbar(structData.wire.(name).x, structData.wire.(name).Avg,...
        structData.wire.(name).Err,markers(i,:),'LineWidth',1,...
        'MarkerSize',6,'CapSize',10)%, 'Color',cmap(i,:));
end

wireLegend = rmmissing(wireLegend);
xlabel('Distance from distal tip [cm]')
ylabel('Flexural rigidity [N·cm^2]')
set(gca,'FontName','Arial','FontSize', 8)
colororder(newColor)
legend(wireLegend,'location','northeastoutside','FontSize', 8)
exportgraphics(gca, 'WireStacked.jpg','Resolution',300)
hold off

%% Zoomed Wires

zoomedwiredims = [0 0 56.896 46.228];
figure('Position',floor(zoomedwiredims./mm_pix))
hold on
wirefieldnames = fieldnames(structData.wire);
for i = 1:length(wirefieldnames)

    ind = find(strcmp(wirefieldnames,strcat('w',...
```

```matlab
        erase(grouping.Wire(i)," "))));

    name = wirefieldnames{ind};
    wireLegend(i) = structData.wire.(name).Name;
    errorbar(structData.wire.(name).x, structData.wire.(name).Avg,...
        structData.wire.(name).Err,markers(i,:),'LineWidth',0.5,...
        'MarkerSize',3,'CapSize',5)%, 'Color',cmap(i,:));
end
xlim([0 20]);
ylim([0 3]);
xlabel('Distance from distal tip [cm]')
ylabel('Flexural rigidity [N·cm^2]')
set(gca,'FontName','Arial','FontSize', 7)
colororder(newColor)

%% Catheters

cathdims = [0 0 180 50];
figure('Position',floor(cathdims./mm_pix))
hold on
catheterfieldnames = fieldnames(structData.catheter);
for i = 1:length(catheterfieldnames)

    ind = find(strcmp(catheterfieldnames,strcat('c',...
        erase(grouping.Catheter(i)," "))));

    name = catheterfieldnames{ind};
    cathLegend(i) = structData.catheter.(name).Name;
    errorbar(structData.catheter.(name).x, ...
        structData.catheter.(name).Avg, ...
        structData.catheter.(name).Err,markers(i,:),'LineWidth',1,...
        'MarkerSize',6,'CapSize',10)
end
cathLegend = rmmissing(cathLegend);
```

```matlab
xlabel('Distance from distal tip [cm]')
ylabel('Flexural rigidity [N·cm^2]')
set(gca,'FontName','Arial','FontSize', 8)
colororder(newColor)
legend(cathLegend, 'Location','eastoutside','FontSize', 8)
exportgraphics(gca,'CatheterStacked.jpg','Resolution',300)
hold off


%% Long Sheaths

lsdims = [0 0 180 50];
figure('Position',floor(lsdims./mm_pix))
hold on
longSheathfieldnames = fieldnames(structData.longSheath);
for i = 1:length(longSheathfieldnames)
    ind = find(strcmp(longSheathfieldnames,strcat('ls',erase(grouping.LongSheath(i)," ")
    name = longSheathfieldnames{ind};
    sheathLegend(i) = structData.longSheath.(name).Name;
    errorbar(structData.longSheath.(name).x, ...
        structData.longSheath.(name).Avg, ...
        structData.longSheath.(name).Err,markers(i,:),'LineWidth',...
        1,'MarkerSize',6,'CapSize',10)
end
sheathLegend = rmmissing(sheathLegend);
xlabel('Distance from distal tip [cm]')
ylabel('Flexural rigidity [N·cm^2]')
set(gca,'FontName','Arial','FontSize', 8)
colororder(newColor)
legend(sheathLegend,'Location','eastoutside','FontSize', 8)
exportgraphics(gca,'longSheathStacked.jpg','Resolution',300)
hold off
```